Mecp2 Fine-tunes Quiescence Exit by Targeting Nuclear Receptors

Jun Yang[1, #], Shitian Zou[2, #], Zeyou Qiu[2, #], Mingqiang Lai[2, #], Qing Long[2], Huan Chen[2], Pinglin Lai[1], Sheng Zhang[2], Zhi Rao[1], Xiaoling Xie[2], Yan Gong[2], Anling Liu[3, *], Mangmang Li[2, *], Xiaochun Bai[1, 2*]

[1] Guangdong Provincial Key Laboratory of Bone and Joint Degenerative Diseases, The Third Affiliated Hospital of Southern Medical University, Guangzhou, 510630, China

[2] State Key Laboratory of Organ Failure Research, Department of Cell Biology, School of Basic Medical Sciences, Southern Medical University, Guangzhou, 510515, China.

[3]Department of Biochemistry, School of Basic Medical Sciences, Southern Medical University, Guangzhou, 510515, China.

[#] These authors contributed equally to this work.

[*]Correspondence: aliu@smu.edu.cn (A.-L.L.), mangmangli@smu.edu.cn (M.-M.L.) and baixc15@smu.edu.cn (X.-C.B.)

Running Title: Mecp2 fine-tunes Quiescence-proliferation balance.

Abstract

Quiescence (G0) maintenance and exit are crucial for tissue homeostasis and regeneration in mammals. Here, we show that methyl-CpG binding protein 2 (Mecp2) expression is cell cycle-dependent and negatively regulates quiescence exit in cultured cells and in an injury-induced liver regeneration mouse model. Specifically, acute reduction of Mecp2 is required for efficient quiescence exit, as deletion of Mecp2 accelerates, while overexpression of Mecp2 delays quiescence exit, and forced expression of Mecp2 after Mecp2 conditional knockout rescues cell cycle reentry. The E3 ligase Nedd4 mediates the ubiquitination and degradation of Mecp2, and thus facilitates quiescence exit. Genome-wide study uncovered the dual role of Mecp2 in preventing quiescence exit by transcriptionally activating metabolic genes while repressing proliferation-associated genes. Particularly, disruption of two nuclear receptors (NRs), *Rara* or *Nr1h3*, accelerates quiescence exit, mimicking the Mecp2 depletion phenotype. Our studies unravel a previously unrecognized role for Mecp2 as an essential regulator of quiescence exit and tissue regeneration.

Keywords: Mecp2, G0 exit, Liver Regeneration, Nedd4

Introduction

Cellular quiescence, also referred to as G0, is a reversible non-proliferating state. Quiescent cells can be reactivated to exit from the quiescent state and reenter the actively cycling states (G1, S, G2 and M phases) in response to certain intrinsic or extrinsic signals. Increasing evidence indicates that quiescence is not a passive non-proliferating state but is rather an active metabolic state maintained by certain transcriptional programs[1,2]. The switch from

quiescence to proliferation is coupled with extensive changes in the transcriptional program coordinating metabolic and proliferation dynamics. The tightly orchestrated quiescence exit is crucial for tissue homeostasis and regeneration after injury, especially in the liver, which is composed of hepatocytes with both metabolic and regenerative capacities[3]. The unique regenerative capability of hepatocytes as differentiated cells after injury makes the liver an ideal *in vivo* model for studying the molecular mechanisms underlying quiescence exit. Recent studies have demonstrated that hepatocytes act like stem cells that possess regenerative potential to reenter the cell cycle and proliferate during liver regeneration[4-6]. Upon quiescence exit, a process also known as priming/initiation, hepatocytes favor proliferative capacity over metabolism to meet the rapid hepatic growth demand. However, how the active metabolic state is transcriptionally altered and modulated during the G0/G1 transition remains to be elucidated.

Methyl-CpG binding protein 2 (Mecp2), as a chromatin-binding protein[7,8], plays multiple roles in gene expression regulation, including transcriptional activation and repression, RNA splicing, chromatin remodeling and regulation of chromatin architecture[9]. Given the high expression and pivotal role of Mecp2 in the brain, understanding the mechanisms of Mecp2 in neurological disorders such as Rett Syndrome and autism has attracted intense interest[8,10,11]. Furthermore, Mecp2 has also been identified as an oncogene highly expressed in several cancer types. Several lines of evidence suggest that the role of Mecp2 in malignancy mainly involves facilitation of cancer cell proliferation and inhibition of apoptosis[12-14]. The role of Mecp2 in quiescence exit and tissue regeneration and the underlying mechanisms have not been reported, to the best of our knowledge.

In this study, using a mouse model of injury-induced liver regeneration and cellular models of quiescence exit, we intriguingly found that Mecp2 is a cell cycle-dependent protein which is drastically abated during the G0/G1 transition and gradually restored at further stages of cell cycle progression. A sharp decline in Mecp2 expression is essential for efficient quiescence exit in response to extrinsic stimuli using both *in vivo* and *in vitro* models. Additionally, the E3 ligase Nedd4 contributes to the ubiquitination and degradation of Mecp2 at quiescence exit, which modulates the pace of quiescence exit. Mechanistically, Mecp2 governs quiescence exit by transcriptionally orchestrating proliferative and metabolic gene expression, among which many nuclear receptor genes (NRs) emerge as novel Mecp2-activated genes in quiescent cells. Together, our findings identify a critical negative regulatory role for Mecp2 in quiescence exit and tissue regeneration, partially through targeting several NRs.

Results

Mecp2 is dynamically expressed during injury-induced liver regeneration

To screen for key regulators governing the initiation/priming phase of liver regeneration, we used the 2/3 partial hepatectomy (PHx) mouse model, a widely used *in vivo* model to study quiescence exit[15]. Surprisingly, Mecp2, a well-known essential regulator of brain development, emerged as a dramatically repressed protein at the priming/initiation stage of PHx-induced liver regeneration. The expression kinetics of Mecp2 were examined at both the mRNA and protein levels in liver tissues at six time points after PHx, which cover the three phases of liver regeneration, namely priming/initiation, progression and termination[3] (Figure S1A, Fig S1 source data). The results showed that Mecp2 was remarkably reduced as early as 6 h after

PHx, was further decreased at 12 h and 24 h, but was restored at the 48- and 120-h time points (Figures 1A, 1B, and S1B, Fig 1 source data and Fig S1 source data). The decrease in the active histone mark H3K27ac [16] at the Mecp2 promoter was consistent with the reduced transcriptional activity within 36 h post-PHx (Figure S1C, Fig S1 source data). Notably, Mecp2 protein levels were decreased more dramatically than mRNA, suggesting a posttranslational regulation of Mecp2 at the very early stage of liver regeneration. The early acute reduction of Mecp2 in hepatocytes during liver regeneration, mainly in nuclei, was further validated by immunofluorescence (IF) staining (Figure 1C, Fig 1 source data) and immunohistochemistry (IHC) (Figure 1D, Fig 1 source data). To confirm the quiescence exit-specific reduction of Mecp2 in hepatocytes, we assessed proliferation-associated proteins that are widely used to distinguish the G0 from the G1 phase, including phosphorylated retinoblastoma protein (pRb), Cyclin D1 and Ki67 (Figures 1B and 1D, Fig 1 source data). The phosphorylation states of Rb, including un-phosphorylated, hypo-phosphorylated and hyper-phosphorylated Rb, can reflect G0, early G1 and late G1 phases, respectively[17]. The results showed that pRb was undetectable by 6 h after PHx. Accordingly, Cyclin D1, which mediates the phosphorylation of Rb, was also maintained at extremely low levels during the very early stage of liver regeneration. Several other cyclins important for the G1/S stage (Cyclin E1) and the G2/M stage (Cyclin A2 and B1), were also expressed at low levels, further supporting the negative correlation between the amount of Mecp2 and cell cycle reentry [18,19] (Figure 1B, Fig 1 source data). Moreover, Ki67, a well-known proliferation marker, which is degraded and barely detected in the G0 phase but accumulates during cell proliferation[20,21], showed an inverse correlation with Mecp2 in hepatocytes within 48 h after

PHx (Figure 1D, Fig 1 source data). It is worth noting that the acute reduction in Mecp2 during quiescence exit was gradually restored by 48 to 120 h post-PHx, suggesting the functional involvement of Mecp2 in active cell cycle phases. Together, these findings demonstrate the identification of Mecp2 as a new cell cycle-associated protein, which is highly expressed in quiescent hepatocytes, sharply decreased at the G0/G1 transition, and gradually restored at later stages of cell cycle progression during injury-induced liver regeneration.

Mecp2 negatively regulates quiescence exit during PHx-induced liver regeneration

Given the acute reduction of Mecp2 during hepatocyte quiescence exit, we asked whether Mecp2 prevents the G0/G1 transition. To this aim, we generated hepatocyte-specific Mecp2 conditional knockout mice (Mecp2-cKO) by crossing control mice containing *Loxp* sites flanking exon 2 and 3 of the *Mecp2* gene ($Mecp2^{fl/fl}$) with albumin (Alb)-Cre mice expressing Cre recombinase under the Alb promoter (Figure S2A, Fig S2 source data). The successful Mecp2 depletion in the liver was confirmed by genotyping (Figure S2B, Fig S2 source data) and measuring the amount of Mecp2 at both mRNA and protein levels in $Mecp2^{fl/fl}$ and Mecp2-cKO mice (Figures S2C and S2D, Fig S2 source data). Mecp2-cKO mice were viable and showed no obvious abnormalities in the liver compared to control littermates (Figures S2E-S2G, Fig S2 source data). PHx triggered the decay of Mecp2 in livers at 6 and 48 h after PHx, which reflected the G0/G1 transition and M phase, respectively, in the remaining hepatocytes undergoing the first round of the cell cycle after PHx (Figures 2A-2C, Fig 2 source data). The results of western blotting and corresponding quantification in Mecp2-cKO livers indicated that Mecp2 depletion promoted quiescence exit in hepatocytes after PHx

(Figure 2B, Fig 2 source data). IF staining for Ki67 showed that Mecp2-deficient livers contained more proliferating hepatocytes than controls, further supporting the enhanced G0/G1 transition in Mecp2-cKO mice (Figure 2C, Fig 2 source data). Accordingly, liver regeneration was significantly enhanced at 6, 12, 24 and 48 h after PHx based on the significantly higher liver index in the Mecp2-cKO mice than in the controls (Figure 2D, Fig 2 source data). Therefore, hepatocyte-specific Mecp2 depletion accelerates quiescence exit in injury-induced regenerating livers.

We next tested whether overexpression (OE) of Mecp2 in hepatocytes has an adverse effect on cell cycle reentry after PHx. Intravenous injection of Adeno-associated virus (AAV)-TBG-Mecp2[22] reinforced the levels of Mecp2 in hepatocytes compared to empty vector (EV) control cells (Figures 2E and 2F, Fig 2 source data). Decreased protein levels of pRb and Cyclin D1, as well as lower levels of Ki67 in nuclei from Mecp2-overexpressing hepatocytes were observed within 48 h after PHx (Figures 2F and 2G, Fig 2 source data). Expectedly, Mecp2 OE significantly delayed cell cycle reentry and resulted in a decreased liver index within 24 h after PHx (Figure 2H, Fig 2 source data). Therefore, Mecp2 OE negatively regulates quiescence exit in hepatocytes after PHx.

To further confirm the specificity of Mecp2 on the regulation of quiescence exit, we performed rescue experiments using AAV-mediated Mecp2 OE in Mecp2-cKO livers (Figures 2I and 2J, Fig S2 source data). The restoration of Mecp2 in Mecp2-depleted hepatocytes was accompanied by increased expression of cell cycle regulators and earlier appearance of Ki67 compared to the EV controls (Figures 2J and 2K, Fig 2 source data). In addition, the increased liver index caused by the loss of Mecp2 was significantly compromised by Mecp2 restoration

(Figure 2L, Fig 2 source data). Therefore, forced restoration of Mecp2 rescues Mecp2 loss-induced accelerated quiescence exit.

Notably, the modest but significant changes in liver regeneration caused by the manipulation of Mecp2 in the first 2 days after PHx disappeared 5 days post-PHx (Figures S2H-S2J, Fig S2 source data), indicating the involvement of Mecp2 in not only quiescence exit but also in later stages of cell proliferation. Taken together, our *in vivo* analyses demonstrate that the rapid reduction of Mecp2 in hepatocytes is essential for efficient quiescence exit during injury-induced liver regeneration.

Acute reduction of Mecp2 is universal for quiescence exit in cellular models

We then asked whether the expression pattern of Mecp2 during the quiescence-proliferation transition is universal in cells. To this end, we released three types of cultured cells, including 3T3 mouse embryonic fibroblasts, mouse hippocampal neuronal HT22 cells and human primary umbilical vein endothelial cells (HUVECs), from quiescence induced by two classical signals, i.e., serum starvation (S.S.) and contact inhibition (C.I.) [23]. The cell cycle analysis in 3T3 cells showed that more than 90% of cells resided in the G0/G1 phase in response to S.S. (Figures 3A and 3B, Fig 3 source data) or C.I. (Figures 3F and 3G, Fig 3 source data), indicating the successful induction of quiescence. The expression kinetics revealed that serum restimulation (S.R.)- and/or C.I. loss (C.I.L.)-induced cell cycle reentry of quiescent 3T3 cells resulted in a dramatic decrease in Mecp2 at the G0/G1 transition and its gradual restoration during cell cycle progression, resembling that seen after PHx-induced initiation of hepatocellular regeneration (Figures 3C, 3D, 3H and 3I, Fig 3 source data). The time course of IF staining for Ki67 and Mecp2 showed extremely low levels of Ki67 signals

in nuclei within 6 h after S.R. (Figure 3E, Fig 3 source data) or 24 h after C.I.L. (Figure 3J, Fig 3 source data), further supporting the reduction in Mecp2 at quiescence exit in 3T3 cells. Similar results were obtained in both HT22 cells (Figures S3A-S3H, Fig S3 source data) and HUVECs (Figures S3I-S3P, Fig S3 source data). Taken together, this evidence suggests that the acute reduction in Mecp2 is a general phenomenon at the G0/G1 transition.

Acute reduction of Mecp2 is essential for efficient quiescence exit in cells

To determine whether the functional relationship between acute Mecp2 reduction and quiescence exit also exists in cells other than hepatocytes, we first assessed the effect of siRNA-mediated Mecp2 knockdown (KD) on the S.R.-induced quiescence exit of 3T3 cells (Figure 4A, Fig 4 source data). Western blotting showed that Mecp2 depletion led to an earlier induction of pRb, Cyclin D1, as well as cyclin A, cyclin B, and cyclin E proteins (Figure 4B, S4A, S4C, Fig 4 source data and Fig S4 source data). The accelerated cell cycle reentry in Mecp2 KD cells was also reflected by the earlier appearance of Ki67 (Figure 4C, Fig 4 source data). Additionally, we used Ki67 and propidium iodide (PI) double staining followed by flow cytometry to quantify G0 cells ($Ki67^{-}$ with 2N DNA content) at early time points after quiescence exit with or without Mecp2 depletion. The results showed that Mecp2 KD significantly reduced G0 cells compared to negative control siRNA (NC si)-treated cells after S.R. (Figure 4D, Fig 4 source data). As such, about 70% of control cells and over 90% of Mecp2 KD cells re-entered the cell cycle at 6 h post-S.R., indicating that Mecp2 KD accelerated quiescence exit in 3T3 cells. Thus, enhanced reduction of Mecp2 stimulates exit from quiescence.

We then asked whether increased Mecp2 expression could postpone quiescence exit. To

test this, we forced Mecp2 OE in 3T3 cells through lentiviral transduction (Figures 4E and 4F, Fig 4 source data). Compared to the EV, Mecp2 OE resulted in the delayed quiescence exit phenotype upon S.R., as evidenced by decreased expression of pRb, Cyclin D1, and other cell cycle protein, such as cyclin A2, cyclin B1 and cyclin E1 (Figure 4F, S4B, S4D, Fig 4 source data and Fig S4 source data), delayed induction of Ki67 (Figure 4G, Fig 4 source data), and a two-fold increase in the proportion of cells residing in the G0 phase (Figure 4H, Fig 4 source data). Notably, neither Mecp2 KD nor OE significantly affected the number of G0 cells without S.R. (Figures 4D and 4H, Fig 4 source data), suggesting that Mecp2 functions upon receiving extracellular mobilization signals. Taken together, these results indicate that acute Mecp2 reduction at the G0/G1 transition is required for efficient quiescence exit.

Nedd4 contributes to Mecp2 degradation and regulates quiescence exit

Given the more rapid decay of Mecp2 at the protein compared to the mRNA level during the quiescence-proliferation transition, we speculated that Mecp2 is targeted by posttranslational regulation. This hypothesis was supported by proteasome inhibition with the proteasome inhibitor MG132, which attenuated the reduction of Mecp2 in quiescent cells after S.R (Figure S5A, Fig S5 source data). In contrast, the lysosome inhibitor chloroquine had no impact on the degradation of MeCP2 protein (Figure S5B, Fig S5 source data). To identify proteins that regulate Mecp2 degradation during the G0/G1 transition, we performed immunoprecipitation followed by mass spectrometry (IP-MS) using Mecp2 antibody in quiescent 3T3 cells treated with or without S.R. (Figure S5C, Fig S5 source data). A total of 647 proteins were identified as putative Mecp2 interactors. We were particularly interested in the proteins involved in proteasome-mediated ubiquitin-dependent protein catabolic process

which was one of the enriched Gene Ontology (GO) items in the Mecp2 interactome (Table S1). Among the candidate genes, we identified the ubiquitin ligase ‘‘neuronal precursor cell developmentally downregulated 4-1’’ (Nedd4) that specifically interacted with endogenous Mecp2 by reciprocal IP-WB in 3T3 cells (Figure 5A, Fig 5 source data). Co-IP using Mecp2 antibody revealed that Mecp2-associated ubiquitin and Nedd4 were dramatically increased at 3 h and 6 h post-S.R. (Figure 5B, Fig 5 source data), suggesting that Nedd4 interacts with Mecp2 to induce the polyubiquitination and degradation of Mecp2 upon cell cycle reentry.

Given the important role of Nedd4 in posttranslational regulation of Mecp2, we reasoned that despite regulating internalization of major growth factor receptors involved in liver regeneration[24], Nedd4-mediated degradation of Mecp2 may be a new mechanism through which Nedd4 contributes to liver regeneration. To test this hypothesis, we assessed the effects of Nedd4 on S.R.-induced quiescence exit of 3T3 cells. Knocking down Nedd4 using siRNA replenished the remarkable reduction of Mecp2 at the early stages of quiescence exit, and thus resulted in lower levels of proliferation markers such as pRb, Cyclin D1 and Ki67 (Figures 5C-5E, Fig 5 source data). Nedd4 deficiency significantly retained cells in the G0 phase upon S.R. (Figure 5F, Fig 5 source data). On the contrary, Nedd4 OE significantly enhanced the degradation of Mecp2 and accordingly accelerated the quiescence exit which mimicked the effect of Mecp2 depletion (Figures 5G-5J, Fig 5 source data). Thus, Nedd4 interacts with Mepc2 and regulates quiescence exit partially through posttranslational regulation of Mecp2 upon quiescence exit.

Mecp2 slows quiescence exit by transcriptionally activating metabolism-associated genes while repressing proliferation-associated genes

It has been well established that Mecp2 transcriptionally regulates gene expression by binding methylated CpG islands and chromatin proteins in the brain [7,25,26]. However, little is known about the transcriptional targets of Mecp2 during hepatocyte quiescence exit in the regenerating liver. To decipher the molecular mechanisms underlying Mecp2-regulated quiescence exit, we performed RNA-seq combined with chromatin immunoprecipitation followed by next generation sequencing (ChIP-seq) to identify the Mecp2-dependent transcriptome genome-wide during the very early stage of liver regeneration (Figure S6C, Fig S6 source data). RNA-seq and comparative analyses in control Mecp2$^{fl/fl}$ and Mecp2-cKO mice livers before and 6 h after PHx revealed 3048 Mecp2-dependent genes that were differentially expressed in a Mecp2-dependent manner. Meanwhile, we mapped the binding landscape of Mecp2 in Mecp2$^{fl/fl}$ livers before and after PHx using ChIP-seq by filtering out peaks identified in Mecp2-cKO livers (Figure S6C, Fig S6 source data). It has been reported that Mecp2 occupies a large proportion of the genome in the brain due to its methyl-CpG (mCpG) binding preference[7,26,27]. Similarly, we identified a total of 14640 and 15350 Mecp2-binding genes before and after PHx in the Mecp2 control liver, respectively (Figures S6A and S6B, Fig S6 source data). To further identify putative Mecp2-direct target genes, we integrated Mecp2-dependent genes with Mecp2-binding genes (Figures S6C, Fig S6 source data). As a result, there were 2658 Mecp2 direct target genes, in which 537 were PHx-activated and 2121 were PHx-repressed genes (Figure 6A, Fig 6 source data). GO analysis showed that PHx-activated Mecp2 targets, which are either silent or basally expressed in quiescent hepatocytes, were highly enriched in proliferation-associated biological processes such as ribosome biogenesis, rRNA metabolic process, ncRNA metabolic

process, and regulation of transcription by RNA polymerase I, whereas PHx-repressed Mecp2 targets, which are highly expressed in quiescent hepatocytes, were associated with several metabolic processes including carboxylic acid catabolic process, cellular amino acid metabolic process, fatty acid metabolic process and steroid metabolic process (Figure 6B, Fig 6 source data). Notably, among PHx-repressed genes, several NRs were newly identified as Mecp2 direct targets, such as *Nr2f6*, *Nr3c1*, *Nr1h3*, *Nr1i3*, *Nr6a1*, *Rxrg*, *Rara*, *Nr4a1*, *Srebf1* and *Ppard* (Figure 6A, Fig 6 source data). To gain insights into the relevance between Mecp2 occupancy and the differential expression of Mecp2 direct targets, we interrogated the binding strength of Mecp2 in the promoter-proximal regions (within 3 kb of the transcription start sites (TSS)) and defined gene regions (±25 kb around the TSS and transcription end sites (TES)) (Figure S6A, Fig S6 source data). Intriguingly, Mecp2 occupancy at these regions was not apparently altered after PHx, which was inconsistent with its protein levels, suggesting that the majority of Mecp2 is not tightly associated with the genome in quiescent hepatocytes and Mecp2 may recruit other factor(s) to achieve the differential transcriptional outcomes in response to extrinsic stimuli (Figure 6C, Fig 6 source data).

Because the liver is a key metabolic organ, we paid particular attention to Mecp2-regulated NRs, whose alteration may result in a shift in the balance between metabolism and proliferation. The Mecp2-dependent transcriptional repression of ten NRs upon hepatic resection was validated using real-time qPCR in both Mecp2 control and cKO livers (Figure 6D, Fig 6 source data). Notably, the mRNA levels of NRs were significantly higher in Mecp2$^{fl/fl}$ than in Mecp2-cKO livers before PHx, suggesting that Mecp2 contributes to the transcriptional activation of NRs in normal livers while Mecp2 degradation upon PHx

leads to their deactivation. We also confirmed the repression of NRs in S.R.-induced 3T3 cell quiescence exit (Figure S6D, Fig S6 source data). We did not detect the expression of *Nr1i3* and *Rxrg* in quiescent 3T3 cells either before or after G0 exit, and failed to validate the repression of *Nr4a1*, suggesting that Mecp2-mediated transcriptional repression of NRs may vary with cell type and/or mobilization signals. Thus, these results suggest that Mecp2 plays a negative regulatory role during quiescence exit by activating metabolism-associated genes while repressing proliferation-associated genes in quiescent cells.

Abolishing Mecp2-activated NRs promotes G0/G1 transition *in vitro* and *in vivo*

To interrogate the functional relevance of Mecp2-mediated repression of NRs to quiescence exit, we selected two candidate genes for further investigation, *Rara* and *Nr1h3*. Retinoic acid (RA) has long been recognized as a liver mitogen required for normal liver regeneration [28]. Rara and Rarb as receptors for RA have been recently identified to mediate RA-induced hepatocyte proliferation after PHx[29]. Cholesterol is another important regulator of cell proliferation. Nr1h3 (LXR) is highly expressed in the liver, and has recently been reported to reduce hepatocyte proliferative capacity during PHx-induced regeneration by regulating genes involved in lipid and cholesterol homeostasis [30,31]. We first performed ChIP-qPCR to confirm the significantly decreased binding intensity of Mecp2 at proximal promoter regions of both *Rara* and *Nr1h3* upon exit quiescence (Figure 7A, Fig 7 source data). Using lentivirus-mediated gene knockdown, we then tested whether individual disruption of two candidate NRs might affect S.R.-induced quiescence exit in 3T3 cells (Figure 7B, Fig 7 source data). The results of western blotting showed that depletion of either *Nr1h3* or *Rara* significantly accelerated the G0/G1 transition, as measured by the expression of pRb and

Cyclin D1 (Figure 7C, Fig 7 source data) and by flow cytometry (Figure 7D, Fig 7 source data), mimicking the Mecp2 KD phenotype. Therefore, Mecp2 prevents quiescence exit, at least in part, by repressing Rara and Nr1h3.

We then asked whether depletion of Rara or Nr1h3 can further promote quiescence exit in Mecp2-cKO livers. We performed AAV-mediated gene knockdown to target *Rara* and *Nr1h3* in Mecp2-cKO livers using short hairpin RNAs (shRNAs) (Figure 7E, Fig 7 source data). Because of the limited number of cKO animals, we could only assess the effects at 6 h post-PHx. The results showed that knockdown of either *Rara* or *Nr1h3* in combination with Mecp2-cKO can modestly but significantly further accelerate quiescence exit during PHx-induced liver regeneration (Figures 7F-7H, Fig 7 source data). Therefore, for the first time to the best of our knowledge, this study has revealed a positive correlation between the repression of Mecp2-activated NRs and quiescence exit, and has identified novel roles of Rara and Nr1h3 in regulating quiescence exit *in vitro* and *in vivo*.

Discussion

The accurate transition from quiescence to the active cell cycle is crucial for the control of eukaryotic cell proliferation and adult stem cell-mediated tissue homeostasis and regeneration after injury. Conversely, dysregulation of quiescence exit may compromise tissue integrity and lead to oncogenesis. In this work, we sought to explore the general molecular mechanisms that regulate quiescence by focusing on Mecp2, a multifunctional protein with a broad spectrum of activities. Using genetic mouse models, cellular models, and genome-wide approaches, we uncovered a regulatory capacity of Mecp2 in quiescence exit (Figure 7I, Fig 7 source data). In quiescent cells, Mecp2 is maintained at relative high levels and serves as both

a transcriptional activator and repressor. It binds to and activates metabolic genes, such as several NRs, while repressing proliferation-associated genes in quiescent and metabolically hyperactive hepatocytes. In response to extrinsic stimuli, such as injury and mitogenic stimulation, the protein levels of Mecp2 are acutely decreased by both transcriptional repression and Nedd4-mediated ubiquitination. The remarkable reduction of Mecp2 releases the transcriptional repression of proliferation-associated genes while compromising the activation of metabolic genes, in order to satisfy a rapidly regenerating demand of the remaining hepatocytes, eventually leading to quiescence exit and cell cycle progression. The transient repression of Mecp2 during quiescence exit and its restoration during further cell cycle progression probably serve as means to avoid over-inhibition of metabolism and to guarantee the appropriate metabolic adaption required for cell proliferation. Therefore, our results suggest that quiescent cells employ Mecp2 to balance the needs of cell division and metabolism upon receiving extrinsic signals.

Although it has been reported that Mecp2 null mice develop fatty liver[32], the Mecp2-cKO mice used in our study did not demonstrate obvious abnormalities, such as necrosis or liver damage when we performed PHx (Figure S2, Fig S2 source data). Based on our comparative analysis of RNA-seq data from control and Mecp2 cKO livers before PHx, only 90 upregulated and 128 downregulated genes (log2 $|FC| > 1.5$, $p < 0.05$) were identified which did not enrich any GO terms with adjusted $p < 1\times10^{-3}$, further supporting the notion that liver-specific deletion of Mecp2 does not cause liver abnormalities in 3-month-old mice. This allowed us to study liver regeneration in mice with non-damaged livers and avoid any defects prior to injury. It is worth noting that, other than accelerated cell cycle reentry, Mecp2

cKO hepatocytes also displayed a modest increase in cell size with enlarged nuclei relative to control cells (Figure S2G, Fig S2 source data), implying the attenuation of mitosis.

It has been well documented that both overexpression and depletion of Mecp2 have deleterious effects on neuronal homeostasis[33], and thus, tight regulation of Mecp2 protein levels is critical for its physiological functions. In addition, several studies have demonstrated that many Rett Syndrome-causing mutations in the methyl-CpG binding domain not only compromise DNA binding capacity of Mecp2 but also reduce its protein stability, implying the relevance of protein stability in Mecp2 dysfunction[8,34,35]. Mecp2 has been shown to undergo various post-translational modifications, including phosphorylation, acetylation, ubiquitination and sumoylation, which may also affect protein stability[36]. Protein degradation via ubiquitination is the most prevalent recycling machinery used by cells. Despite 11 identified ubiquitination sites in Mecp2, our knowledge about the E3 ligases that catalyze the covalent attachment of ubiquitin to these sites remains scarce[37,38]. Recently, Wang et al. uncovered the role of RING Finger Protein 4 (RNF4) in transcriptional activation by mediating the ubiquitination of Mecp2[39]. Herein, we discovered Nedd4 as a novel regulator of Mecp2 protein stability. Nedd4 has recently been identified as an essential regulator of liver regeneration through posttranslational modification of growth factor signaling[24]. Consistent with our results, Bachofner et al. reported *in vivo* knockdown of Nedd4 in hepatocytes caused inhibition of cell proliferation after PHx. Although we identified Nedd4-mediated ubiquitination of Mecp2 in the cellular model of quiescence exit, we also measured the expression of Nedd4 at the early stages of liver regeneration (Figure S5D, Fig S5 source data), which in turn may drive hepatocytes to enter the cell cycle by targeting Mecp2. Further

studies are needed to explore what domain(s) is (are) responsible for the interaction between Mecp2 and Nedd4, which corresponding ubiquitylation sites within Mecp2 are targeted by Nedd4, and whether ubiquitylation site mutations of Mecp2 can completely abolish cell cycle reentry.

The switch from quiescence to active cycling requires coordinating all the necessary metabolic and cell cycle machinery. There is an urgent need to synthesize DNA, proteins and lipids required for the generation of daughter cells in resting cells reentering the cell cycle [40]. Regarding injury-induced hepatic regeneration, a global transcriptome shift from metabolism to proliferation is a reasonable strategy to satisfy the proliferating needs at the early stages of liver regeneration after PHx[41]. Consistently, we observed an increase in gene expression involved in mRNA abundance, splicing and translation, and a decrease in genes enriched in fatty acid, lipid, and amino acid metabolism at 6 h post-PHx in a Mecp2-dependent manner (Figures 6A and 6B, Fig 6 source data). This metabolic repression is transient and largely restored when the regenerating liver reaches its original size. Yet, how Mecp2 differentially regulates proliferation-associated and metabolic genes is a fascinating question that remains unanswered in our study and merits further investigation.

In this study, we discovered that Mecp2-mediated transcriptional activation of genes involved in metabolism is one of the mechanisms which prevents exit from quiescence. Specifically, we identified ten NRs, which are ligand-dependent transcription factors that regulate cellular metabolism, proliferation, differentiation, and apoptosis. The NR superfamily can be divided into three classes based on their ligands and mechanisms of action, including the steroid receptor family, the thyroid/retinoid family and the orphan receptor family[42-44]. To

date, studies on NRs have elucidated the roles of several NRs in regulating hepatomegaly and liver regeneration, including peroxisome proliferator-activated receptors (PPARα or Nr1c1, and PPARγ or Nr1c3), pregnane X receptor (PXR, Nr1i2), constitutive androstane receptor (CAR, Nr1i3), liver X receptor (LXR, Nr1h3) and farnesoid X receptor (FXR, Nr1h4)[45]. Among these genes, *Nr1i3* and *Nr1h3* also emerged as PHx-repressed Mecp2-activated NRs in our study. Consistent with our observations, Sasso et al. demonstrated that Nr1h3, which is responsible for cholesterol catabolism and fatty acid synthesis, acts as an inhibitor of liver regeneration[30]. However, they did not observe the decreased mRNA levels of both LXR isoforms (Nr1h3 and Nr1h2), mainly because they monitored the transcriptional levels at one day post-PHx, which was not early enough to capture the upstream changes in transcriptional regulation. In general, previous studies have barely focused on the connection between quiescence exit and NRs. Based on our observations, the inhibition of certain NRs by Mecp2 depletion during quiescence exit is probably general and not hepatocyte-specific, because we also validated the repression of several NRs in cellular models of quiescence exit. Additionally, the functional validation of Nr1h3 and Rara in 3T3 cells further supports the notion that Mecp2 may postpone cell cycle reentry through activating NRs. However, not all NRs exhibit the same function in quiescence exit. Huang and colleagues reported that the absence of the primary nuclear bile acid receptor FXR (also known as Nr1h4) strongly inhibited liver growth in the early stages of regeneration[46]. Therefore, the cell type- and/or stimulus-specific function and detailed mechanisms for certain NRs in regulating quiescence exit await further investigation. Our study highlights the importance of NRs in mediating Mecp2-regulated quiescence exit, which may serve as attractive therapeutic targets after

further investigation of the underlying mechanisms.

In summary, our study opens a brand-new perspective to understand the functional involvement of Mecp2 as a general regulator of quiescence exit, and has provided insight into the mechanisms that may link metabolism to quiescence exit. Differential targeting of Mecp2 based on its different roles at different cell-cycle phases should be taken into consideration when examining potential clinical applications.

Methods

Resources Table

Detailed information for reagents, antibodies, primers, and shRNAs were listed in the Resources Table

Experimental animals

All the animal research protocols were in accordance with the U.S. Public Health Service Policy on Use of Laboratory Animals and were approved by the Ethics Committee on Use and Care of Animals of Southern Medical University. All the animal studies were performed in accordance with the ethical guidelines of South Medical University ethics committee. Ten- to 12-week-old female C57BL/6 mice were purchased from the Laboratory Animal Centre of Southern Medical University (Guangzhou, China). The *Alb*-cre (JAX stock #025200) mouse strain was obtained from Jackson Laboratory (Bar Harbor, ME, USA). Mecp2$^{flox/flox}$ (#NM-CKO-190001) mice were obtained from Shanghai Model Organisms Center (Shanghai, China). To generate hepatocyte-specific *Mecp2* knockout mice by the deletion of exon 2 and exon 3, we mated *Mecp2*$^{flox/flox}$ mice with *Alb*-Cre^{+} mice to obtain *Alb*$^{+}$*Mecp2*$^{flox/+}$ female mice. The *Alb*$^{+}$*Mecp2*$^{flox/+}$ female mice were then bred with *Mecp2*$^{flox/}$Y male mice to obtain

Alb^{+}*Mecp2*$^{flox/\ flox}$ female mice (termed Mecp2 cKO) and littermate controls (*Alb*$^{-}$*Mecp2* $^{flox/\ flox}$). All mice were housed at 22°C under a 12-hour light/dark cycle. Food and water were provided *ad libitum*. Genotyping was carried out on tail DNA by polymerase chain reaction (PCR) using specific primers, and Mecp2 deficiency in hepatocytes was confirmed via WB and Q-PCR.

Partial hepatectomy surgery

For standard two-thirds PHx, 10–12-week-old mice were used in this study. Surgery was performed using methodology described previously between 9:00 and 12:00 AM[15]. The mice were then euthanatized with pentobarbital at specified time points. To study the expression of Mecp2 in cell cycle progression, tissue was harvested at time points representing the G1 phase (6, 12 and 24 h after PH), S/G2 phase (48 h after PH), and the 'post-replicative' phase of liver regeneration (120 h after PH). Livers from non-operated mice served as G0 phase (PHx 0 h) controls. At the specified time points, livers were fixed in 10% buffered formalin for 24 h or frozen in liquid nitrogen for later experiments. Liver and body weights were recorded at the time of death for calculating liver-to-body weight ratios.

Cell culture and synchronization

NIH3T3 and HUVEC cells were obtained from American Type Culture Collection (Manassas, VA, USA), and the HT22 cells were purchased from the Procell Life Science Technology (Wuhan, China). All cells were cultured in DMEM (Gibco, Grand Island, NY, # C11995500) containing 4.5 g/l glucose and 10% fetal bovine serum (Thermo Fisher Scientific, USA, #10438026). To synchronize cells in G0 by S.S., cells were plated at a density of 1 x 10^4 cells per cm^2 overnight and allowed to attach to the tissue culture plate. Cells were washed three

times with phosphate-buffered saline and starved in DMEM with 0.1% FBS for 30 h[23]. Afterwards, the cells were induced into the cell cycle with 15% FBS and collected at the indicated times.

For cells arrested by C.I., cells were plated at high density (1 x 10^5 cells/cm^2), grown to confluence and maintained at confluence for up to 3 days[47]. During this time, the cells undergo C.I. entering G0 arrest. The G0-phase cells were then plated at a density of 2 x 10^4 cells per cm^2 and cultured with 10% FBS. After attachment, cell samples were collected at 24, 48 and 72 h. Subsequent analyses using qPCR, WB, IF and cell cycle analysis were performed.

FACS cell cycle profile analysis

Cell-cycle phases were monitored by flow cytometry, as previously described[20]. The cells in different cell cycle phases were harvested and fixed overnight at 4°C with 70% ethanol. The following day, the fixed cells were centrifuged at 250 g for 5 min, and the pellet was resuspended in 1 mL PBS, centrifuged, and resuspended in 1 mL propidium iodide (PI) staining solution containing RNase A (CST, MA, USA, #4087). After incubation at room temperature for 30 min in the dark, DNA content profiles were obtained via flow cytometry using a FACScan instrument. Gates were set over the G0/G1, S and G2/M peaks, and then the percentages of cells in different cell cycle phases were calculated.

For Ki67 expression, PI-labeled cells were stained with Ki-67-APC antibody (Biolegend, San Diego, CA, USA, # 652406) for 30 min at room temperature. Ki67 level and DNA content profiles were analyzed via flow cytometry. The percentage of cells in the G0 phase was defined as Ki-67^- and PI^+ (2 N)[20]. Flow cytometry data were analyzed with FlowJo V10

(FlowJo, USA).

mRNA extraction and quantitative RT–PCR

Cells and liver samples were homogenized in 1.0 ml of TRIZOL. RNA was isolated using chloroform extraction and transcribed into cDNA using Prime Script Reverse Transcriptase (Takara, Shiga, Japan, #2680B) at 1000 ng in a total volume of 20 μl following the manufacturer's protocol. A volume of 2 μl of cDNA was used as template for qPCR using SYBR Premix Ex Taq (Takara, Shiga, Japan, #RR420A). qPCR reactions were performed using an ABI 7500 system (Applied Biosystems, Foster City, CA, USA). Samples were normalized for expression levels of human or mouse actin. The comparative ΔΔCt method was used to quantify the relative fold changes and β-actin mRNA served as an internal control. The specific primers sequences used are listed in Resources Table.

RNA-seq data analysis

Total RNAs from control and Mecp2-KO mice at PHx 0 h and PHx 6 h were performed by Novogene (Beijing, China). The integrity of RNA was assessed using the RNA Nano 6000 Assay Kit of the Bioanalyzer 2100 system (Agilent Technologies, CA, USA). After the fragmentation was carried out, first strand cDNA was synthesized using random hexamer primer and M-MuLV Reverse Transcriptase, then use RNaseH to degrade the RNA. Second strand cDNA synthesis was performed using DNA Polymerase I and dNTP. The library fragments were purified with AMPure XP system (Beckman Coulter, Beverly, USA) and then sequenced by the Illumina NovaSeq 6000. According to the Eoulsan pipeline[48], data were processed using read filters, mappings, alignment filters, read quantifications, normalizations and differential analyses. Before mapping, polyN read tails were trimmed, reads ≤ 40 bases

were removed, and reads with quality mean ≤ 30 were discarded. Alignments from reads matching more than once on the reference genome were removed using the Java version of samtools[49]. All overlapping regions between alignments and referenced exons (or genes) were counted using HTSeq-count[50]. The normalization step and the differential analyses were carried out with DESeq2[51]. RNA-seq reads were aligned to the mouse genome (mm10). $P < 0.05$ and foldchange ≥ 1.5 were set as the thresholds for significantly differential expression.

ChIP and ChIP-seq

ChIP assays were performed using the SimpleChIP Plus Enzymatic Chromatin IP Kit (CST, MA, USA, #9005) according to the procedures provided by the manufacturer. Liver tissues were harvested at the indicated time and quickly cut into ~0.2 cm^3 pieces, crosslinked with 1% formaldehyde for 15 min and quenched with 2.5 M glycine for 5 min at room temperature. After centrifugation, the pieces were homogenized in ice-cold PBS first with a loose pestle and then with a tight pestle, permeabilized and re-suspended in micrococcal nuclease (MNase) buffer and incubated with MNase for 20 min at 37°C. The MNase-digested chromatin was centrifuged at 14,000 rpm for 1 min. Afterwards, the cells were resuspended in ChIP buffer and the chromatin was sonicated on ice (30 s on/30 s off) to obtain soluble sheared chromatin (average DNA length of 150–450 bp). Approximately 10 µg of chromatin was diluted in ChIP buffer and pre-cleared with Dynabeads Protein G (Invitrogen, 10004D) for 2 h at 4°C. Anti-H3K27ac antibodies (5 µg, Abcam, Cambridge, UK, ab4729) and anti-Mecp2 antibodies (8 µg, Abcam, Cambridge, UK, ab2828) were added to the pre-cleared chromatin, followed by rotation overnight at 4°C. The Dynabeads were washed with low/high salt solutions and eluted twice in TE buffer containing 1% SDS at 65°C for 15 min. The combined eluates were

isolated by reversal of cross-linking, incubated with RNase A (10 μg/ml) followed by proteinase K (0.1 mg/ml), and the DNA was extracted using a phenol-chloroform extraction protocol. DNA quality was assessed using an Agilent (Santa Clara, CA, USA) bioanalyzer and quantified using a Qubit fluorometer.

Afterward, the immunoprecipitated chromatin DNA was sent to Novogene Company (Novogene, Beijing, China) for ChIP-seq. Reads coming from Mecp2 were trimmed using Trimmomatic[52] and aligned to the mouse genome (mm10) using Bowtie2[53], followed by processing using Samtools[49]. Peak calling was performed using MACS for narrow peaks[54] and HOMER for broad peaks[55], and peak annotation was performed using HOMER. Aligned reads were normalized using deepTools[56]. By using the normalized BigWig files of ChIP and input samples, the averaged signal was quantified by big Wig Summary, and the ratio of ChIP/input was used as the ChIP signal intensity.

ChIP-qPCR

H3K27ac and Mecp2 were assessed in promoters of genes of interest by ChIP-qPCR. ChIP-DNA from the liver was obtained as described above. Protein-bound DNA was amplified by qPCR. Data were then normalized to the input and expressed as fold-changes (relative enrichment) compared with the control group. Normal rabbit IgG (CST, MA, USA, #2729) serve as the negative control. qPCR analyses of immunoprecipitated chromatin were performed for promoter sequences within +2.5 kb of the transcription start site of analyzed genes. Percentage of input was then calculated for ChIP-qPCR signals. Promoter-specific primers used for these studies are listed in Resources Table.

WB analysis

Mouse tissues or cell cultures were lysed in RIPA buffer (50 mM Tris–HCl pH 7.4, 1% NP-40, 0.25% Na-deoxycholate, 150 mM NaCl, 1 mM EDTA pH 7.4) containing a cocktail of protease inhibitors (Roche, #4693132001) and phosphatase inhibitors (Roche, #4906837001), followed by centrifugation at 10,000 *g* for 10 min at 4°C. The supernatant protein quantity was determined using a BCA assay (Thermo Fisher Scientific, MA, USA, #23235) Equal amounts of protein (30 μg) were resolved by electrophoresis in a 10% or 12% gel and transferred to nitrocellulose membranes (GE Healthcare, Westborough, MA, #88018). The membranes were then incubated with specific antibodies. The membranes were then visualized by enhanced chemiluminescence using an ECL Kit (PerkinElmer, MA, USA #0RT2655). Using Image J software, the values of the target protein/β-actin were calculated to evaluate the relative protein level.

siRNA knockdown

We transiently transfected NIH3T3 cells with Mecp2 or Nedd4 siRNA (Genema, Shanghai, China) using Lipofectamine 3000 (Thermo Fisher Scientific, MA, USA, #L3000-015) in Opti-MEM medium, according to the manufacturer's instructions. Transfected cells were arrested in G0 by 30-h S.S., then collected following 15% FBS stimulation for 3 or 6 h. The effects of knock-down were evaluated by qPCR and WB. Subsequent analyses for IF and cell cycle analysis were also performed. The specific sequences used are listed in Resources Table.

Gene overexpression experiments

NIH3T3 cells were transfected with Mecp2 (Origene, CA, USA, #MR226839, #MR207745) or Nedd4 (Origene, CA, USA, #MR222243) plasmid using Lipofectamine 3000 in serum-free

medium for 12 h, then the medium was removed and replaced with DMEM containing 10% FBS for 24 h. Transfected cells were arrested in G0 for 30 h by serum starvation, then collected followed by 15% FBS re-stimulation for 3 or 6 h. Empty PCMV6-Entry vector was used as a control. The efficacy of overexpression was analyzed by RT-qPCR and WB analysis. Subsequent analyses for IF and cell cycle analysis were also performed.

Histological staining and IHC

Murine liver biopsies were processed for histological analysis. The liver samples were fixed in 4% paraformaldehyde at room temperature for 24 h, embedded in paraffin and stained for histological analysis. After removal of paraffin, hematoxylin-eosin (H&E) staining was performed using a Hematoxylin and Eosin Staining Kit (Beyotime, Shanghai, China, #C0105S). For immunohistochemistry (IHC) staining, sections from liver biopsies were treated with citrate antigen retrieval solution for 3 min by high-pressure. After blocking in 10% goat serum for 60 min at room temperature, the sections were processed for Mecp2 (CST, MA, USA, #3456, 1:100) and Ki67 (CST, MA, USA, #12202, 1:200) using diaminobenzidine according to the manufacturer's instructions.

IF

To evaluate the expression of Mecp2 or Ki67 during the phase of liver generation, primary antibodies, including anti-Alb (Proteintech, Wuhan, China, #66051-1-Ig, 1:200), anti-Mecp2 (CST, MA, USA, #3456, 1:100) or anti–Ki67 (Abcam, Cambridge, UK, #ab279653, 1:100) were added to sections for 12 h at 4°C. Sections were washed three times in PBS, followed by application of secondary antibody goat anti-mouse Alexa Fluor 488 (Thermo Fisher Scientific, MA, USA, #A21202, 1:200) or donkey anti-rabbit Alexa Fluor 594 (Thermo Fisher Scientific,

MA, USA, #A21207, 1:200) at a 1:200 dilution for 1 h at room temperature. Nuclei were counterstained using DAPI (Thermo Fisher Scientific, MA, USA, #D-1306). Following a wash in PBS, tissues were mounted with 50% glycerol and viewed on a Nikon (Tokyo, JP) Eclipse epi-fluorescence microscope.

IF procedures were performed as follows: G0 and cell cycle re-entry NIH3T3 cells were fixed with 4% paraformaldehyde and then washed twice with PBS. Cells were then permeabilized with 0.2% Triton X-100 at 4°C for 15 min and subsequently blocked with 1% BSA for 60 min at room temperature. Primary antibodies included anti-Mecp2 (CST, MA, USA, #3456, 1:100), anti-Nedd4 (Proteintech, Wuhan, China, #21698-1-AP, 1:100) and anti-Ki67 (Abcam, Cambridge, UK, #ab279653, 1:100), which were incubated overnight at 4°C in the presence of 1% BSA. The cells were then visualized using secondary antibody conjugated to Alexa Fluor-488 (Thermo Fisher Scientific, MA, USA, #A21202) or Alexa Fluor-594 (Thermo Fisher Scientific, MA, USA, #A21207) as described above.

Ubiquitination

To determine whether the Mecp2 protein was degraded by proteases during the phase of cell cycle re-entry, NIH3T3 cells were synchronized by S.S. for 30 h, collected following stimulation by 15% FBS with or without 10 μM MG132 (Selleck Chemicals, Houston, TX, USA; #S2619) for 3 or 6 h, and subjected to WB. Endogenous protein in the Mecp2 ubiquitination assay was examined by IP. The cellular lysates of G0 and cell cycle re-entry-cells were lysed in IP lysis buffer (Thermo Fisher Scientific, MA, USA, #87787), and the supernatant was obtained by centrifugation at 10000 × *g* for 10 min at 4 °C. One mg of total protein was incubated with anti-Mecp2 (5 μg) antibody overnight at 4 °C with

constant mixing. Then, antigen-antibody complexes were incubated with magnetic beads for 2 h with shaking. After three washings, retained proteins were eluted using 30 μl of SDS lysis buffer. Eluted Mecp2-associated cellular proteins were separated by SDS-PAGE. Ubiquitination was analyzed using anti-ubiquitin antibody (CST, MA, USA, #3936, 1:1000).

Co-IP assay

NIH3T3 cells were synchronized in G0 phase by S.S. as previously described, followed by 15% FBS stimulation for 3 or 6 hours. Cells were washed with cold PBS and lysed in IP lysis buffer supplemented with protease inhibitors (Roche, Basel, Switzerland, #05892791001). The supernatant was obtained by centrifugation at 10000 × *g* for 10 min at 4 °C. Protein concentrations were quantified using a BCA Protein Assay Kit (Thermo Fisher Scientific, MA, USA, #23250). One milligram of total protein was incubated with anti-Mecp2 (5 μg) or anti-Nedd4 (5 μg) antibody overnight at 4 °C with constant mixing. Then, 30 μl of Dynabeads (Thermo Fisher Scientific, MA, USA, #10004D) were added and incubation was continued for an additional 2 h. After three washings with PBS, retained proteins were eluted using 30 μl of SDS lysis buffer. Protein complexes were then detected by WB and then immunoblotted with anti-Mecp2 or Nedd4 antibodies.

Mass spectrometry assay

To reveal the proteins of the ubiquitination system possibly interacting with Mecp2, NIH3T3 cells were synchronized by S.S. for 36 hours and collected following 15% FBS stimulation for 3 or 9 hours. Total protein (1 mg) was incubated with anti-Mecp2 (5 μg) overnight at 4 °C with constant mixing. IgG was used as the negative control. Then, antibody was incubated with Dynabeads for 2 h with shaking. After three washings, retained proteins were

eluted using 30 μl of SDS lysis buffer. Eluted Mecp2-associated cellular proteins were separated by SDS-PAGE and stained with Coomassie blue. Trypsin was used to digest stained protein bands. An Orbitrap Elite mass spectromete was used to analyze the digested samples by Applied Protein Technology Co., Ltd. (Shanghai, China). Using Mascot as a search engine, fragment spectra were scanned against the Uniprot database to identify proteins. In this assay, Nedd4 was identified as the most abundant peptide of E3 ligase during the G0-G1 transition.

Lentiviral vector constructs and transduction

For stable knockdown of Nr1h3 and Rara, lentiviruses were generated according to our previous protocol[57]. Briefly, shRNAs targeting luciferase or mouse Nr1h3 and Rara were cloned into the pLKO.1 vector (Addgene, MA, USA, #8453). The lentiviral vectors were co-transfected with the packaging vectors pCMV-deltaR8 (Addgene, MA, USA, #12263) and pCMV-VsVg (Addgene, MA, USA, #8454) into LentiX-293T cells to generate virus. After 48 h, virus was collected and used to infect NIH3T3 cells with 6 μg/ml polybrene (Sigma, St Louis, MO, USA; #TR-1003) for another 12 h. Infected cells were selected in puromycin (4 μg /ml) for 3 days, and the expression of Nr1h3 and Rara in infected cells was verified by qRT–PCR. We used pLKO.1-luciferase-Puro empty vector as a negative control. The sequences of the shRNAs are listed in Resources Table.

AAV production and tail vein injection

In vivo Mecp2 overexpression was achieved by recombinant adeno-associated virus serotype 8 (AAV8) vectors. AAV8 vectors carrying Mecp2 or GFP sequences with a TBG (thyroxin-binding globulin) promoter (AAV8-TBG-GFP, AAV8-TBG-Mecp2) were manufactured by Genechem Co., Ltd (Shanghai, China). AAV8-TBG-GFP served as negative

control. AAV8-TBG-GFP/Mecp2 vectors (2×10^{11} vector genomes per mouse) were injected intravenously into C57 mice (termed AAV-Mecp2 mice) or $CKO^{Alb\text{-}Mecp2}$ mice (termed Mecp2 cKO/AAV-Mecp2 mice), respectively. After 4 weeks, 70% PHx was performed as described above. Mecp2 overexpression were verified by IF and WB. The remaining livers were collected at 6 and 48 h after surgery. Liver-to-body weight ratios were calculated as described above.

To knockdown the expression of Nr1h3 or Rara in Mecp2-KO mice, AAV8-mediated delivery of shRNAs was used in this study. The vehicle vector ssAAV-TBG-mNeonGreen-WPRE-SV40pA was used as a negative control (termed shLuc). AAV production was performed according to our previous method[57]. Briefly, 293T cells were co-transfected with various plasmids. We transfected 40 μg of total DNA (5.7 μg of pAAV8, 11.4 μg of pHelper (ZoomaBio, #ZK736) and 22.8 μg of TBG-NeonGreen-mir30-shNr1h3 (termed shNr1h3) or 22.8 μg of TBG-NeonGreen-mir30-shRara (termed shRara) into 293T cells in a 15-cm dish. After 12 h, the transfection medium was changed to normal medium. The medium containing AAV was collected at 72 h and 120 h post-transfection, and the cells were collected at 120 h post-transfection. AAV particles were digested from cells by salt-active nuclease (ArcticZymes, Sweden, #70910-202). Subsequently, AAV vector particles were purified by ultracentrifugation in an iodixanol density gradient at 350,000 *g* for 2 h at 18°C. The virus titer was determined by real-time PCR. AAV vector (2×10^{11} vector genomes per mouse) were injected intravenously via the tail vein to Mecp2 cKO mice. After 4 weeks, 70% PHx was performed as described above. The knockdown efficacy of Nr1h3 and Rara was verified by qPCR. The remaining livers were collected 6 h after surgery. Liver-to-body

weight ratios were calculated as described above.

Table S1 for the GO enrichment analysis the binding proteins of Mecp2 during the cell cycle re-entry.

Accession Numbers

ChIP-seq and mRNA-seq data have been submitted to the GEO repository under accession number GSE227727 and GSE227723. The mass spectrometry proteomics data have been deposited to the *ProteomeXchange* Consortium and are available via *ProteomeXchange* (PXD042085).

Statistics

Statistical significance in each group was analyzed by Student's t-test, one-way ANOVA or two-way ANOVA.

Acknowledgments

This work was supported by grants from the National Natural Science Foundation of China (31900507, 92268204), the Guangdong Basic and Applied Basic Research Foundation (2019A1515011511) and the China Postdoctoral Science Foundation (2019M652955, 2023M731541).

Author Contributions

X.-C.B., M.-M.L. and A.-L.L. designed the study; J.Y., S.-T.Z., Q.L., M.-Q.L., P.-L.L., S.Z., Z.R., X.-L.X., and Y.G. performed experiments; H.C cloned lentiviral vector; Z.-Y.Q. and M.-M.L. performed the bioinformatics analysis.

Declaration of Interests

The authors declare no competing interests.

Figure Legends

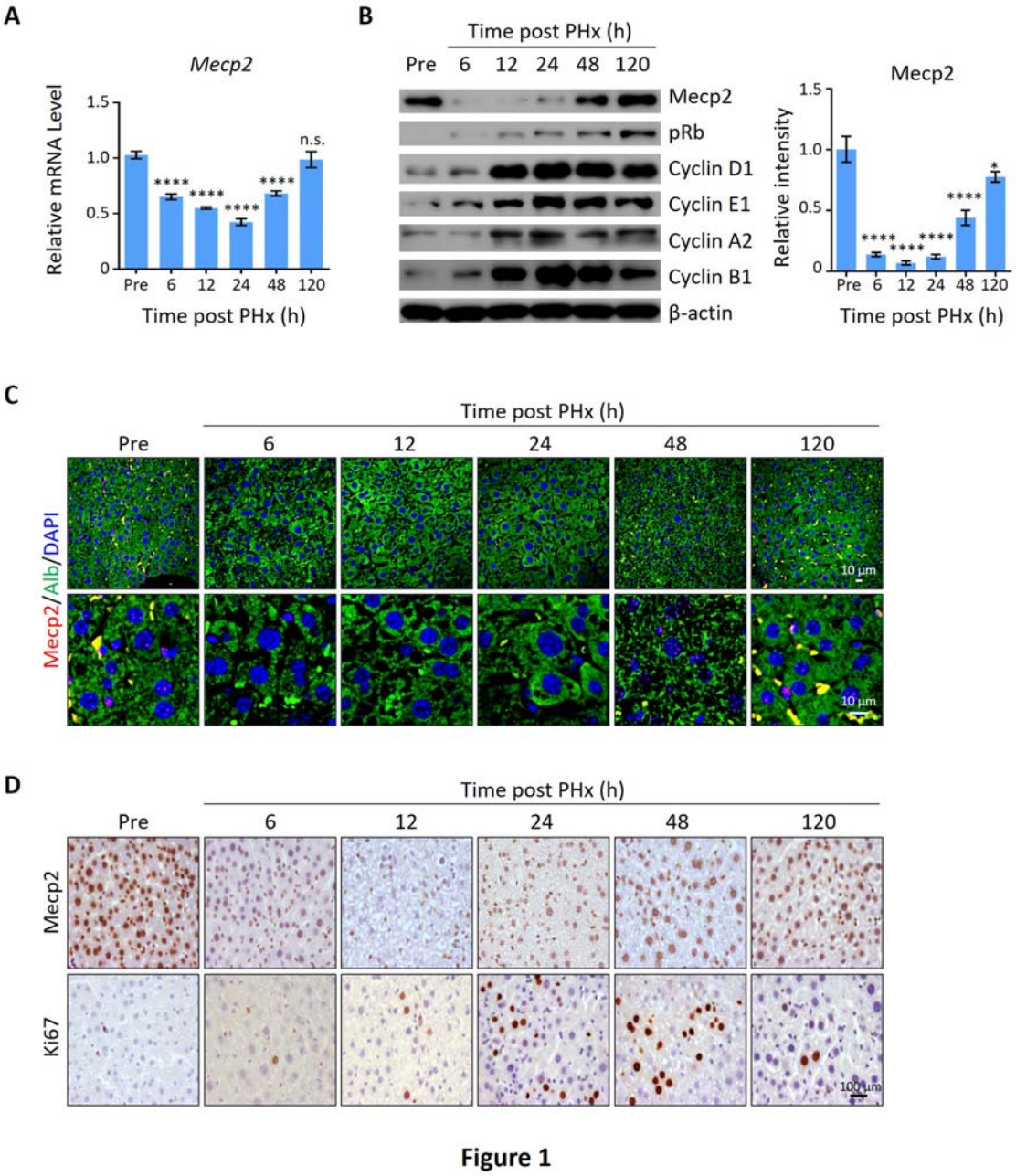

Figure 1. Mecp2 is immediately decreased in the liver after PHx.

(A) Real-time PCR to evaluate mRNA levels of Mecp2 at different time points after PHx. Data are presented as means ± SEM; n = 6. n.s., not significant; ****$p < 0.0001$ by one-way ANOVA.

(B) WB showing the time course of protein levels of Mecp2, pRb, Cyclin D1, Cyclin E1, Cyclin A1, Cyclin B1 and β-actin in mouse livers after PHx. Right panel, quantification of Mecp2. Data are presented as means ± SEM; n = 3. n.s., not significant; ****$p < 0.0001$; *$p < 0.05$ by one-way ANOVA.

(C) Representative IF staining of Mecp2 (red) and Alb (green), together with DAPI (blue) for nuclei in liver sections at different time points after PHx. Lower panels, higher-magnification images.

(D) Representative IHC images of liver tissues stained for Mecp2 or Ki67 at the indicated time points after PHx.

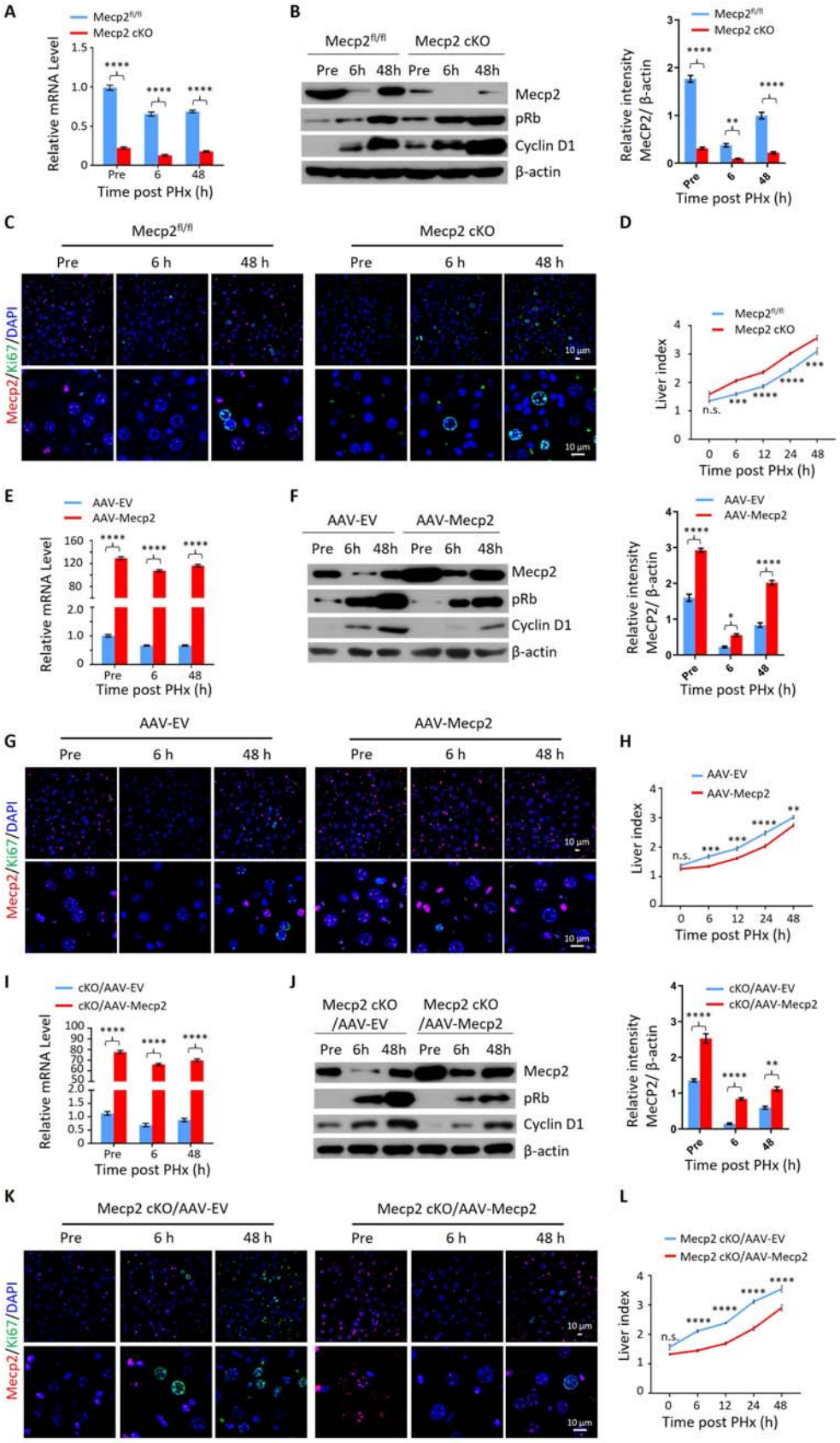
A
Mecp2fl/fl
Mecp2 cKO
Relative mRNA Level
Time post PHx (h)
B
Mecp2fl/fl
Mecp2 cKO
Pre 6h 48h Pre 6h 48h
Mecp2
pRb
Cyclin D1
β-actin
Relative intensity MeCP2/ β-actin
Time post PHx (h)
C
Mecp2fl/fl
Mecp2 cKO
Pre 6 h 48 h
Mecp2/Ki67/DAPI
10 μm
D
Liver index
Time post PHx (h)
E
AAV-EV
AAV-Mecp2
Relative mRNA Level
Time post PHx (h)
F
AAV-EV
AAV-Mecp2
Pre 6h 48h Pre 6h 48h
Mecp2
pRb
Cyclin D1
β-actin
Relative intensity MeCP2/ β-actin
Time post PHx (h)
G
AAV-EV
AAV-Mecp2
Pre 6 h 48 h
Mecp2/Ki67/DAPI
10 μm
H
Liver index
Time post PHx (h)
I
cKO/AAV-EV
cKO/AAV-Mecp2
Relative mRNA Level
Time post PHx (h)
J
Mecp2 cKO /AAV-EV
Mecp2 cKO /AAV-Mecp2
Pre 6h 48h Pre 6h 48h
Mecp2
pRb
Cyclin D1
β-actin
Relative intensity MeCP2/ β-actin
Time post PHx (h)
K
Mecp2 cKO/AAV-EV
Mecp2 cKO/AAV-Mecp2
Pre 6 h 48 h
Mecp2/Ki67/DAPI
10 μm
L
Liver index
Time post PHx (h)

Figure 2

Figure 2. Mecp2 fine-tunes quiescence exit in hepatocytes after PHx *in vivo*.

(A-D) Liver regeneration in Mecp$^{fl/fl}$ and Mecp2 cKO mice after PHx. (A) Real-time PCR to measure mRNA levels of *Mecp2*. The effects and corresponding quantification of Mecp2 KO on quiescence exit and liver regeneration were assessed by WB of Mecp2, pRb and Cyclin D1 (B), IF staining of Mecp2 (red) and Ki67 (green) in liver sections (C), and liver index of control and Mecp2 cKO mice (D) at the indicated time points.

(E-H) Liver regeneration in Mecp2$^{fl/fl}$ livers without (AAV-EV) or with AAV-mediated Mecp2 OE (AAV-Mecp2) after PHx. EV, empty vector. (E) Real-time PCR to measure mRNA levels of *Mecp2*. (F-H) The effects and corresponding quantification of Mecp2 OE on quiescence exit and liver regeneration were assessed by WB of Mecp2, pRb and Cyclin D1 (F), IF staining of Mecp2 (red) and Ki67 (green) in liver sections (G), and liver index at the indicated time points (H).

(I-L) Liver regeneration in Mecp2 cKO livers without (Mecp2 cKO/AAV-EV) or with AAV-mediated Mecp2 restoration (Mecp2 cKO/AAV-Mecp2) after PHx. (I) Real-time PCR to measure mRNA levels of *Mecp2*. (J-L) The effects and corresponding quantification of Mecp2 restoration on quiescence exit and liver regeneration in Mecp2 cKO livers were assessed by WB of Mecp2, pRb and Cyclin D1 (J), IF staining of Mecp2 (red) and Ki67 (green) in liver sections (K), and liver index (L) at the indicated time points. Data are presented as means ± SEM. In (A), (E), (I), n=6; (B), (F) (J), n = 3; in (D), (H), and (L), n = 5 mice/group. n.s., not significant; *$p < 0.05$; **$p < 0.01$; ***$p < 0.001$; ****$p < 0.0001$ by two-way ANOVA.

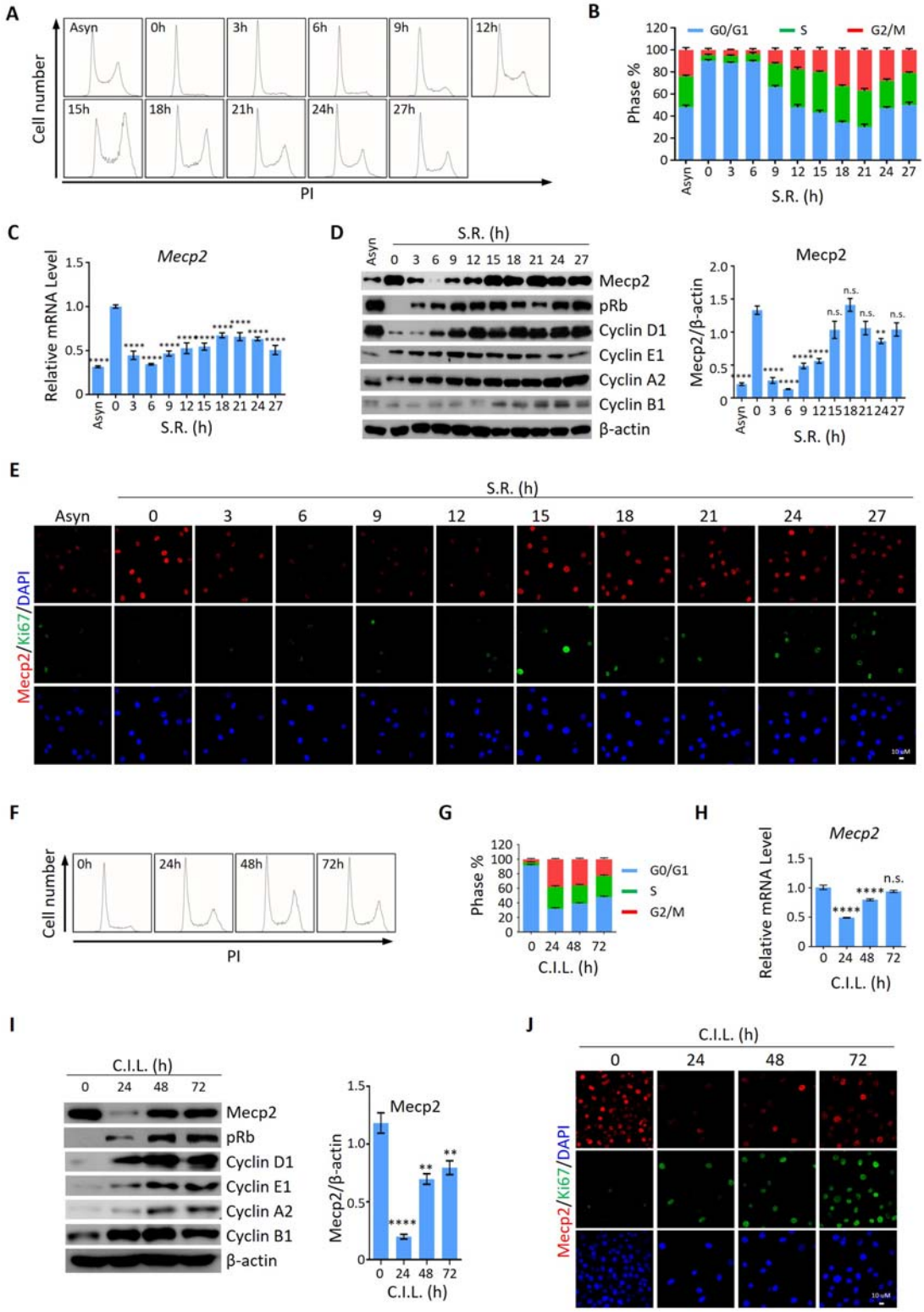

Figure 3

Figure 3. Mecp2 is immediately decreased during quiescence exit in cellular models.

(A-B) Representative histograms of PI staining of either asynchronized (Asyn) proliferating or starvation-induced quiescent 3T3 cells after S.R. in (A) and statistical analysis of cell cycle distribution (B).

(C) Real-time PCR to examine mRNA levels of Mecp2. Data are presented as means ± SEM; n = 9. n.s., not significant; ****$p < 0.0001$ by one-way ANOVA.

(D) WB of Mecp2, pRb, Cyclin D1, Cyclin E1, Cyclin A1 and Cyclin B1 in quiescent 3T3 cells upon S.R.. Right panel, quantification of Mecp2. Data are presented as means ± SEM; n = 3. n.s., not significant; ****$p < 0.0001$ by one-way ANOVA.

(E) Representative IF staining of Mecp2 (red) and Ki67 (green), together with DAPI (blue) in Asyn and quiescent 3T3 cells upon S.R..

(F-G) Representative histograms of PI staining of C.I.-induced quiescent 3T3 cells after C.I.L. (F) and statistical analysis of cell cycle distribution (G) at the indicated time points.

(H) Real-time PCR to examine mRNA levels of *Mecp2* in 3T3 cells released from C.I.-induced quiescence. Data are presented as means ± SEM; n=6. n.s., not significant; ****$p < 0.0001$ by one-way ANOVA.

(I) WB of Mecp2, pRb, Cyclin D1, Cyclin E1, Cyclin A1 and Cyclin B1 in quiescent 3T3 cells upon C.I.L.. Right panel, quantification of Mecp2. Data are presented as means ± SEM; n = 3. n.s., not significant; ****$p < 0.0001$ by one-way ANOVA.

(J) Representative IF staining of Mecp2 and Ki67 in 3T3 cells released from C.I.-induced quiescence. See also Figure S3.

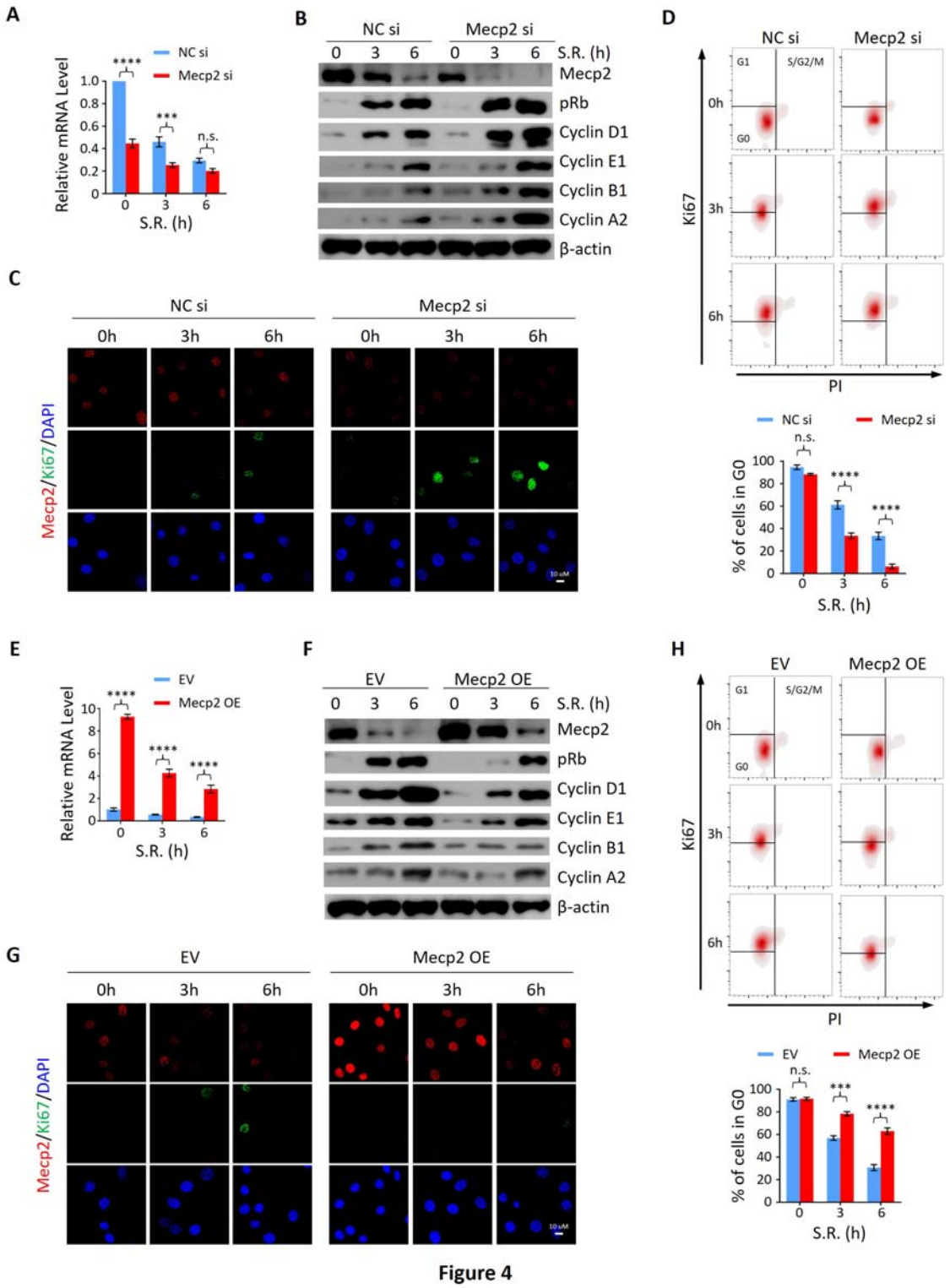

Figure 4. Mecp2 negatively regulates the G0/G1 transition in the cellular model of S.R.-induced quiescence exit.

(A) Real-time PCR showing the mRNA levels of *Mecp2* in 3T3 cells transfected with negative control siRNA (NC si) or Mecp2 siRNA (Mecp2 si) at the early stages of S.R.-induced cell cycle reentry. Data are presented as means ± SEM; n = 6. n.s. not significant; ***$p < 0.001$; ****$p < 0.0001$ by two-way ANOVA.

(B) WB of Mecp2, pRb, Cyclin D1, Cyclin E1, Cyclin A2, Cyclin B1 in control and Mecp2 KD 3T3 cells released from S.S.-induced quiescence at the indicated time points.

(C) Representative IF staining of Mecp2 and Ki67 in control and Mecp2 KD 3T3 cells upon S.R.-induced quiescent exit.

(D) Ki67 and PI double staining followed by flow cytometry showing cell cycle profiles of 3T3 cells transfected with NC or Mecp2 siRNA upon S.R.-induced quiescence exit. Cells in G0, G1 and S/G2/M phases were defined by Ki67−/2N DNA content, Ki67+/2N DNA content and >2N DNA content population, respectively. Lower panel, quantification of the percentage of 3T3 cells in the G0 phase. Data are presented as means ± SEM; n = 3. n.s. not significant; ****$p < 0.0001$ by two-way ANOVA.

(E) Real-time PCR showing the mRNA levels of *Mecp2* in 3T3 cells transduced with the EV or the vector overexpressing Mecp2 (Mecp2 OE) at the early stages of quiescence exit. Data are presented as means ± SEM; n = 3. ****$p < 0.0001$ by two-way ANOVA.

(F) WB of Mecp2, pRb, Cyclin D1, Cyclin E1, Cyclin A2, Cyclin B1 in control and Mecp2 OE 3T3 cells released from S.S.-induced quiescence at the indicated time points.

(G) Representative IF staining of Mecp2 and Ki67 in quiescent control and Mecp2 OE 3T3 cells upon S.R..

(H) Representative flow cytometry plots of Ki67/PI double staining in control and Mecp2 OE

3T3 cells upon S.R.-induced quiescence exit. Lower panel, quantification of proportion of 3T3 cells in the G0 phase. Data are presented as means ± SEM; n = 3. n.s. not significant; ***$p < 0.001$; ****$p < 0.0001$ by two-way ANOVA.

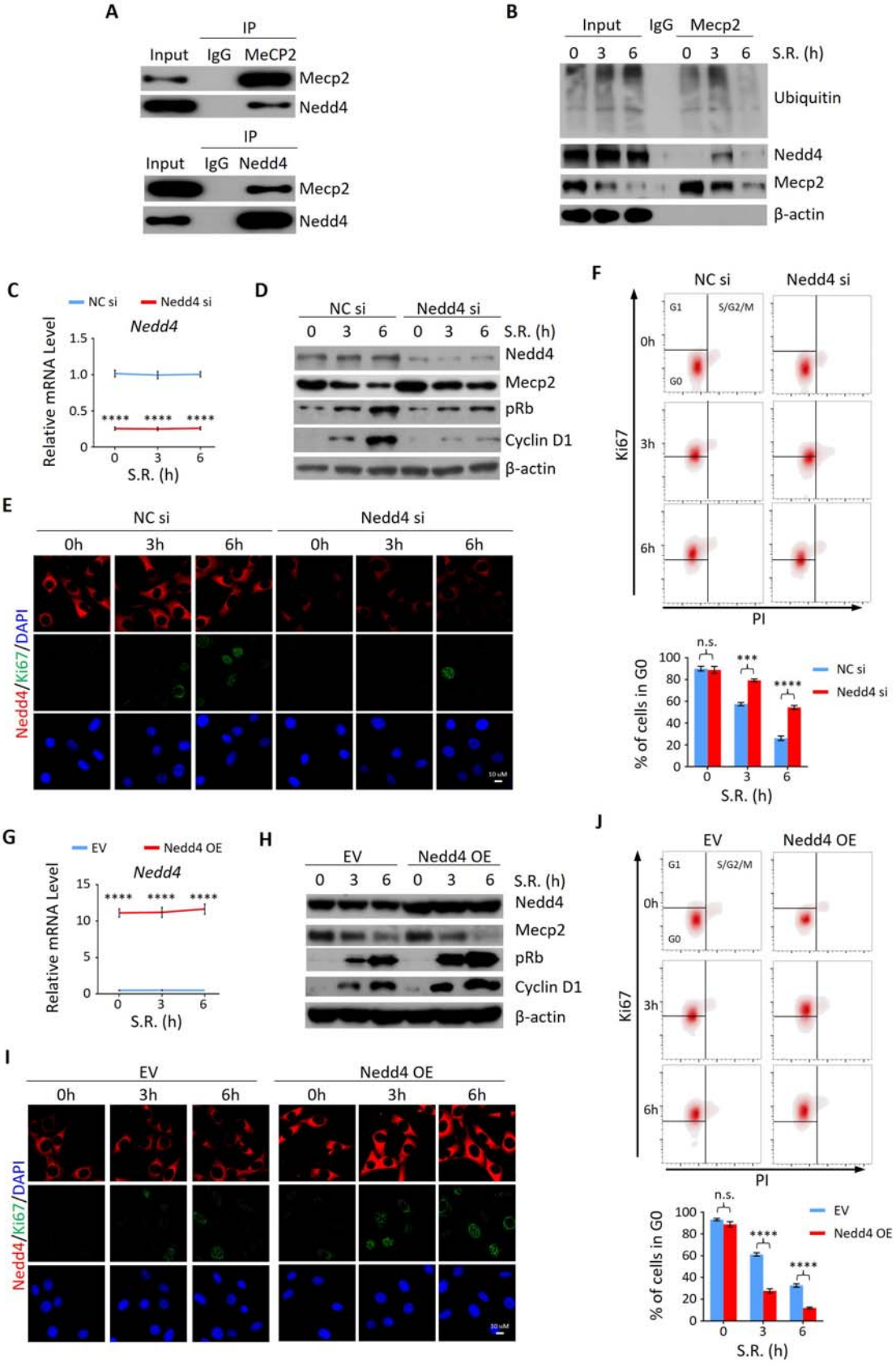
A
IP
Input IgG MeCP2
Mecp2
Nedd4
IP
Input IgG Nedd4
Mecp2
Nedd4
B
Input IgG Mecp2
0 3 6 0 3 6 S.R. (h)
Ubiquitin
Nedd4
Mecp2
β-actin
C
NC si
Nedd4 si
Nedd4
Relative mRNA Level
S.R. (h)
D
NC si Nedd4 si
0 3 6 0 3 6 S.R. (h)
Nedd4
Mecp2
pRb
Cyclin D1
β-actin
E
NC si Nedd4 si
0h 3h 6h 0h 3h 6h
Nedd4/Ki67/DAPI
F
NC si Nedd4 si
G1 S/G2/M
G0
0h 3h 6h
Ki67
PI
% of cells in G0
n.s.
S.R. (h)
G
EV
Nedd4 OE
Nedd4
Relative mRNA Level
S.R. (h)
H
EV Nedd4 OE
0 3 6 0 3 6 S.R. (h)
Nedd4
Mecp2
pRb
Cyclin D1
β-actin
I
EV Nedd4 OE
0h 3h 6h 0h 3h 6h
Nedd4/Ki67/DAPI
J
EV Nedd4 OE
G1 S/G2/M
G0
0h 3h 6h
Ki67
PI
% of cells in G0
n.s.
S.R. (h)

Figure 5

797

Figure 5. Nedd4 interacts with Mecp2 and affects quiescence exit by facilitating Mecp2 degradation.

(A) Reciprocal IP-WB analysis to validate the interaction between endogenous Mecp2 and Nedd4.

(B) Co-IP of Mecp2, ubiquitin and Nedd4 in quiescent 3T3 cells during S.R.-induced quiescence exit.

(C) Real-time PCR showing siRNA-mediated Nedd4 KD in 3T3 cells upon S.R.-induced quiescence exit. Data are presented as means ± SEM; n = 5. ****$p < 0.0001$ by two-way ANOVA.

(D-F) The effect of Nedd4 KD on quiescent exit in 3T3 cells determined by WB (D), IF staining of Ki67 and Nedd4 (E), and Ki67/PI staining followed by flow cytometry (F) at the indicated time points. Lower panel in (F): quantification of the percentage of 3T3 cells in the G0 phase. Data are presented as means ± SEM; n = 3. n.s. not significant; ***$p < 0.001$, ****$p < 0.0001$ by two-way ANOVA.

(G) Real-time PCR showing Nedd4 OE in 3T3 cells upon S.R.-induced quiescence exit. Data are presented as means ± SEM; n = 5. ****$p < 0.0001$ by two-way ANOVA.

(H-J) The effect of Nedd4 OE on quiescent exit in 3T3 cells determined by WB (H), IF staining of Ki67 and Nedd4 (I), and Ki67/PI staining (J) at the indicated time points. Data are presented as means ± SEM; n = 3. n.s. not significant; ****$p < 0.0001$ by two-way ANOVA.

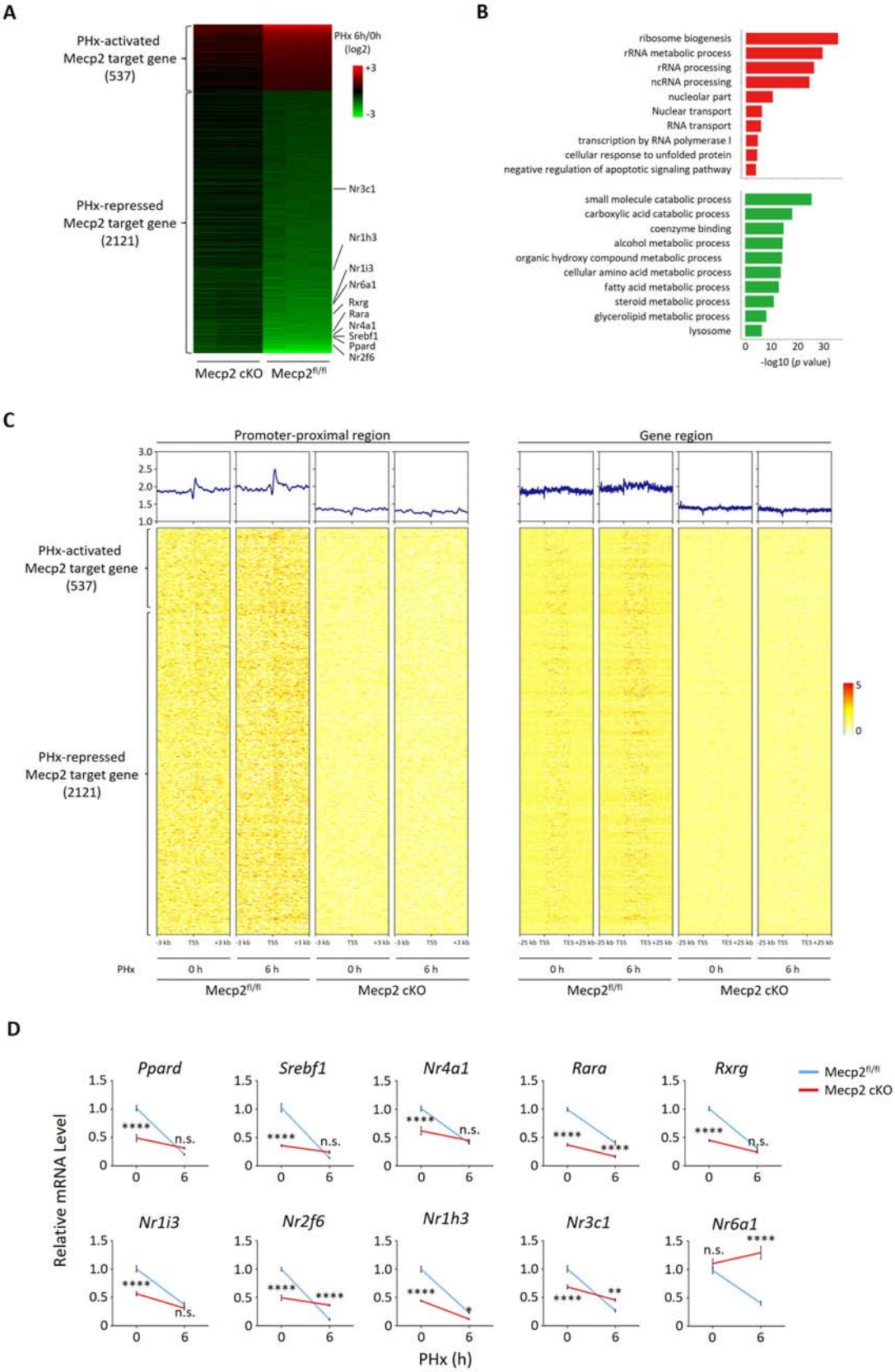
A
PHx-activated
Mecp2 target gene
(537)
PHx-repressed
Mecp2 target gene
(2121)
PHx 6h/0h
(log2)
+3
-3
Nr3c1
Nr1h3
Nr1i3
Nr6a1
Rxrg
Rara
Nr4a1
Srebf1
Ppard
Nr2f6
Mecp2 cKO
Mecp2fl/fl
B
ribosome biogenesis
rRNA metabolic process
rRNA processing
ncRNA processing
nucleolar part
Nuclear transport
RNA transport
transcription by RNA polymerase I
cellular response to unfolded protein
negative regulation of apoptotic signaling pathway
small molecule catabolic process
carboxylic acid catabolic process
coenzyme binding
alcohol metabolic process
organic hydroxy compound metabolic process
cellular amino acid metabolic process
fatty acid metabolic process
steroid metabolic process
glycerolipid metabolic process
lysosome
0 10 20 30
-log10 (p value)
C
Promoter-proximal region
Gene region
PHx-activated
Mecp2 target gene
(537)
PHx-repressed
Mecp2 target gene
(2121)
PHx
0 h
6 h
Mecp2fl/fl
Mecp2 cKO
D
Ppard
Srebf1
Nr4a1
Rara
Rxrg
Nr1i3
Nr2f6
Nr1h3
Nr3c1
Nr6a1
Relative mRNA Level
PHx (h)
Mecp2fl/fl
Mecp2 cKO
****
n.s.
**

Figure 6

Figure 6. Mecp2 transcriptionally regulates quiescence exit.

(A) Heatmap of Mecp2 direct target genes at the early stage of liver regeneration rank-ordered by their gene expression fold change.

(B) The top ten most significantly overrepresented GO terms for the PHx-activated (red) and PHx-repressed (green) Mecp2 target genes.

(C) Heatmaps depicting ChIP-seq enrichment of Mecp2 at the promoter-proximal region (3 kb away from TSS) and the defined gene region of Mecp2 target genes in $Mecp^{fl/fl}$ and Mecp2 cKO livers before and 6 h post-PHx. Genes are rank-ordered according to the fold change of expression.

(D) Real-time PCR validation of PHx-repressed NRs in $Mecp2^{fl/fl}$ and Mecp2 cKO livers upon PHx. Data are presented as means ± SEM; n = 5. n.s. not significant; $^{**}p < 0.01$; $^{****}p < 0.0001$ by two-way ANOVA.

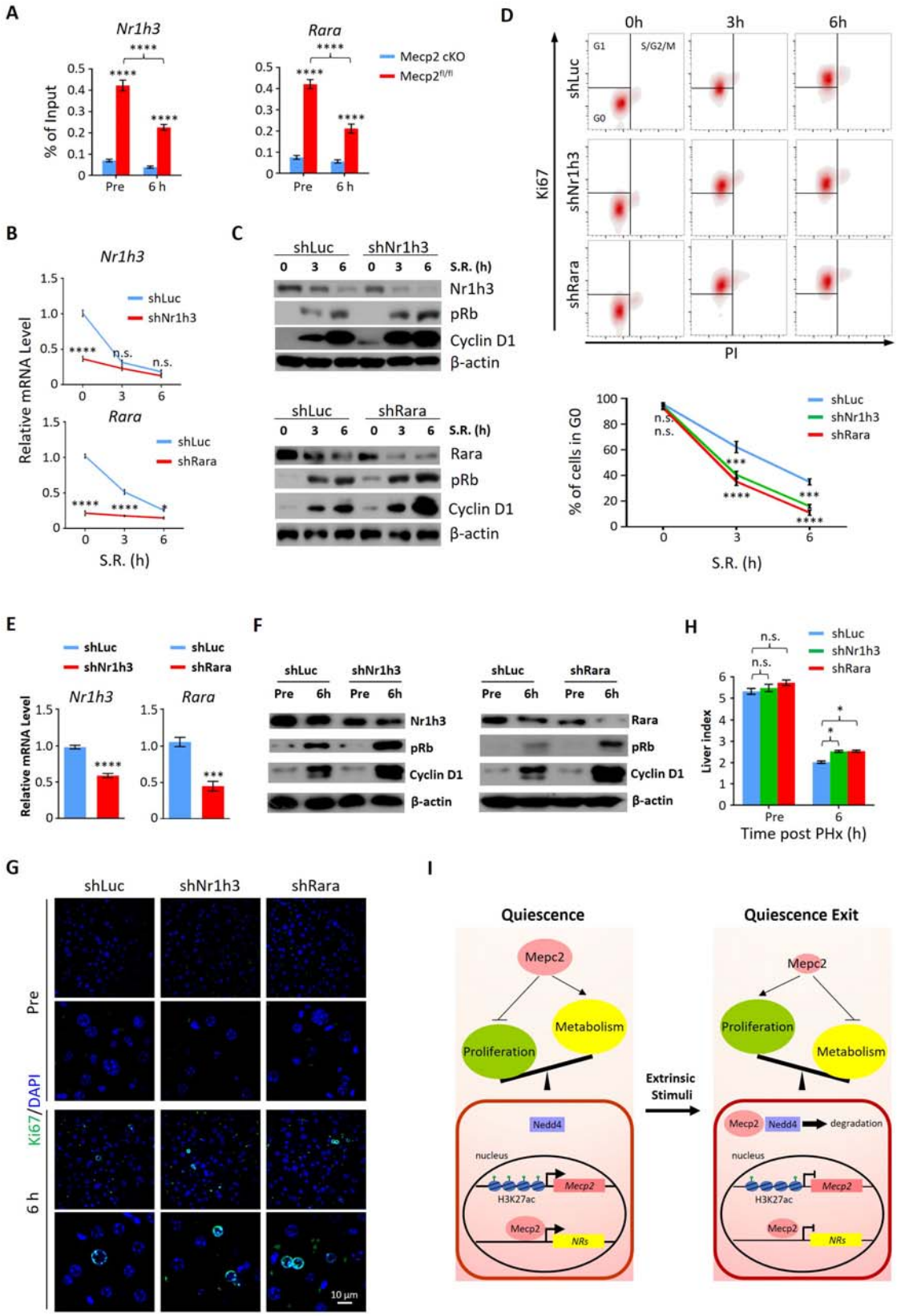
A
Nr1h3
Rara
% of Input
Pre
6 h
Mecp2 cKO
Mecp2fl/fl
B
Nr1h3
Rara
Relative mRNA Level
shLuc
shNr1h3
shRara
n.s.
S.R. (h)
C
shLuc
shNr1h3
shRara
S.R. (h)
Nr1h3
pRb
Cyclin D1
β-actin
Rara
D
0h
3h
6h
G1
S/G2/M
G0
Ki67
PI
% of cells in G0
E
Relative mRNA Level
F
Pre
6h
H
Liver index
Time post PHx (h)
G
Pre
6 h
Ki67/DAPI
10 μm
I
Quiescence
Quiescence Exit
Mepc2
Metabolism
Proliferation
Extrinsic Stimuli
Nedd4
nucleus
H3K27ac
Mecp2
NRs
degradation

Figure 7

Figure 7. Depletion of either Nr1h3 or Rara mimics the Mecp2 KD phenotype during quiescence exit.

(A) ChIP-qPCR analyses of Mecp2 at the promoter-proximal regions of *Rara* and *Nr1h3* in $Mecp2^{fl/fl}$ and Mecp2-cKO livers before and 6 h post-PHx.

(B-D) Either Nr1h3 or Rara KD promotes S.R.-induced quiescence exit in 3T3 cells. (B) Real-time PCR showing lentivirus-mediated knockdown of either *Nr1h3* or *Rara*. shLuc served as a negative control. (C) WB of pRb, Cyclin D1, Nr1h3 and Rara in control and Nr1h3 or Rara KD 3T3 cells at the indicated time points. (D) The effect of Nr1h3 or Rara KD on quiescent exit in 3T3 cells determined by Ki67/PI staining followed by flow cytometry. Data are presented as means ± SEM; In (A) and (B), n = 5; in (D), n = 3. *$p < 0.05$; ***$p < 0.001$; ****$p < 0.0001$ by two-way ANOVA.

(E-H) Either Nr1h3 or Rara KD further enhances quiescence exit in Mecp2 cKO livers. (E) Real-time PCR showing AAV-mediated knockdown of either Nr1h3 or Rara. shLuc served as a negative control. (F) WB of pRb, Cyclin D1, Nr1h3 and Rara in control and Nr1h3 or Rara KD 3T3 cells at the indicated time points. (G) The effect of Nr1h3 or Rara KD on quiescent exit in Mecp2 cKO livers determined by IF and liver index (H) before and 6 h post-PHx. Data are presented as means ± SEM. In (E) and (H), n = 5 mice/group; n.s. not significant; *$p < 0.05$, ****$p < 0.0001$ by two-way ANOVA.

(I) Model of the negative regulatory role for Mecp2 in fine-tuning quiescence exit.

References

1. Roche, B., Arcangioli, B., and Martienssen, R. (2017). Transcriptional reprogramming in cellular quiescence. RNA biology *14*, 843-853. 10.1080/15476286.2017.1327510.
2. Yao, G. (2014). Modelling mammalian cellular quiescence. Interface Focus *4*, 20130074. 10.1098/rsfs.2013.0074.
3. Fausto, N., Campbell, J.S., and Riehle, K.J. (2006). Liver regeneration. Hepatology *43*, S45-53.

10.1002/hep.20969.

4. Michalopoulos, G.K., and Bhushan, B. (2020). Liver regeneration: biological and pathological mechanisms and implications. Nature Reviews Gastroenterology & Hepatology *18*, 40-55. 10.1038/s41575-020-0342-4.

5. Matsumoto, T., Wakefield, L., Tarlow, B.D., and Grompe, M. (2019). In Vivo Lineage Tracing of Polyploid Hepatocytes Reveals Extensive Proliferation during Liver Regeneration. Cell stem cell. 10.1016/j.stem.2019.11.014.

6. Chen, F., Jimenez, R.J., Sharma, K., Luu, H.Y., Hsu, B.Y., Ravindranathan, A., Stohr, B.A., and Willenbring, H. (2019). Broad Distribution of Hepatocyte Proliferation in Liver Homeostasis and Regeneration. Cell stem cell. 10.1016/j.stem.2019.11.001.

7. Lee, W., Kim, J., Yun, J.M., Ohn, T., and Gong, Q. (2020). MeCP2 regulates gene expression through recognition of H3K27me3. Nature communications *11*, 3140. 10.1038/s41467-020-16907-0.

8. Tillotson, R., and Bird, A. (2019). The Molecular Basis of MeCP2 Function in the Brain. J Mol Biol. 10.1016/j.jmb.2019.10.004.

9. Ezeonwuka, C.D., and Rastegar, M. (2014). MeCP2-Related Diseases and Animal Models. Diseases *2*, 45-70. 10.3390/diseases2010045.

10. Ip, J.P.K., Mellios, N., and Sur, M. (2018). Rett syndrome: insights into genetic, molecular and circuit mechanisms. Nat Rev Neurosci *19*, 368-382. 10.1038/s41583-018-0006-3.

11. Guy, J., Cheval, H., Selfridge, J., and Bird, A. (2011). The role of MeCP2 in the brain. Annu Rev Cell Dev Biol *27*, 631-652. 10.1146/annurev-cellbio-092910-154121.

12. Babbio, F., Castiglioni, I., Cassina, C., Gariboldi, M.B., Pistore, C., Magnani, E., Badaracco, G., Monti, E., and Bonapace, I.M. (2012). Knock-down of methyl CpG-binding protein 2 (MeCP2) causes alterations in cell proliferation and nuclear lamins expression in mammalian cells. BMC Cell Biol *13*, 19. 10.1186/1471-2121-13-19.

13. Neupane, M., Clark, A.P., Landini, S., Birkbak, N.J., Eklund, A.C., Lim, E., Culhane, A.C., Barry, W.T., Schumacher, S.E., Beroukhim, R., et al. (2016). MECP2 Is a Frequently Amplified Oncogene with a Novel Epigenetic Mechanism That Mimics the Role of Activated RAS in Malignancy. Cancer discovery *6*, 45-58. 10.1158/2159-8290.CD-15-0341.

14. Zhao, L., Liu, Y., Tong, D., Qin, Y., Yang, J., Xue, M., Du, N., Liu, L., Guo, B., Hou, N., et al. (2017). MeCP2 Promotes Gastric Cancer Progression Through Regulating FOXF1/Wnt5a/beta-Catenin and MYOD1/Caspase-3 Signaling Pathways. EBioMedicine *16*, 87-100. 10.1016/j.ebiom.2017.01.021.

15. Mitchell, C., and Willenbring, H. (2008). A reproducible and well-tolerated method for 2/3 partial hepatectomy in mice. Nature protocols *3*, 1167-1170. 10.1038/nprot.2008.80.

16. Creyghton, M.P., Cheng, A.W., Welstead, G.G., Kooistra, T., Carey, B.W., Steine, E.J., Hanna, J., Lodato, M.A., Frampton, G.M., Sharp, P.A., et al. (2010). Histone H3K27ac separates active from poised enhancers and predicts developmental state. Proceedings of the National Academy of Sciences of the United States of America *107*, 21931-21936. 10.1073/pnas.1016071107.

17. Narasimha, A.M., Kaulich, M., Shapiro, G.S., Choi, Y.J., Sicinski, P., and Dowdy, S.F. (2014). Cyclin D activates the Rb tumor suppressor by mono-phosphorylation. eLife *3*. 10.7554/eLife.02872.

18. Coller, H.A. (2007). What's taking so long? S-phase entry from quiescence versus proliferation. Nature reviews. Molecular cell biology *8*, 667-670. 10.1038/nrm2223.

19. Moser, J., Miller, I., Carter, D., and Spencer, S.L. (2018). Control of the Restriction Point by Rb and p21. Proceedings of the National Academy of Sciences of the United States of America *115*, E8219-E8227. 10.1073/pnas.1722446115.

20. Kim, K.H., and Sederstrom, J.M. (2015). Assaying Cell Cycle Status Using Flow Cytometry. Current

protocols in molecular biology *111*, 28 26 21-28 26 11. 10.1002/0471142727.mb2806s111.

21. Miller, I., Min, M., Yang, C., Tian, C., Gookin, S., Carter, D., and Spencer, S.L. (2018). Ki67 is a Graded Rather than a Binary Marker of Proliferation versus Quiescence. Cell Rep *24*, 1105-1112 e1105. 10.1016/j.celrep.2018.06.110.

22. Greig, J.A., Nordin, J.M.L., Draper, C., McMenamin, D., Chroscinski, E.A., Bell, P., Gray, J.T., Richman, L.K., and Wilson, J.M. (2018). Determining the Minimally Effective Dose of a Clinical Candidate AAV Vector in a Mouse Model of Crigler-Najjar Syndrome. Molecular therapy. Methods & clinical development *10*, 237-244. 10.1016/j.omtm.2018.07.008.

23. Coller, H.A., Sang, L., and Roberts, J.M. (2006). A new description of cellular quiescence. PLoS biology *4*, e83. 10.1371/journal.pbio.0040083.

24. Bachofner, M., Speicher, T., Bogorad, R.L., Muzumdar, S., Derrer, C.P., Hurlimann, F., Bohm, F., Nanni, P., Kockmann, T., Kachaylo, E., et al. (2017). Large-Scale Quantitative Proteomics Identifies the Ubiquitin Ligase Nedd4-1 as an Essential Regulator of Liver Regeneration. Dev Cell *42*, 616-625 e618. 10.1016/j.devcel.2017.07.025.

25. Nan, X., Campoy, F.J., and Bird, A. (1997). MeCP2 is a transcriptional repressor with abundant binding sites in genomic chromatin. Cell *88*, 471-481. 10.1016/s0092-8674(00)81887-5.

26. Rube, H.T., Lee, W., Hejna, M., Chen, H., Yasui, D.H., Hess, J.F., LaSalle, J.M., Song, J.S., and Gong, Q. (2016). Sequence features accurately predict genome-wide MeCP2 binding in vivo. Nat Commun *7*, 11025. 10.1038/ncomms11025.

27. Lagger, S., Connelly, J.C., Schweikert, G., Webb, S., Selfridge, J., Ramsahoye, B.H., Yu, M., He, C., Sanguinetti, G., Sowers, L.C., et al. (2017). MeCP2 recognizes cytosine methylated tri-nucleotide and di-nucleotide sequences to tune transcription in the mammalian brain. PLoS genetics *13*, e1006793. 10.1371/journal.pgen.1006793.

28. Bushue, N., and Wan, Y.Y. (2009). Retinoic Acid-mediated Nuclear Receptor Activation and Hepatocyte Proliferation. J Exp Clin Med *1*, 23-30. 10.1016/S1878-3317(09)60007-3.

29. Liu, H.X., Ly, I., Hu, Y., and Wan, Y.J. (2014). Retinoic acid regulates cell cycle genes and accelerates normal mouse liver regeneration. Biochem Pharmacol *91*, 256-265. 10.1016/j.bcp.2014.07.003.

30. Lo Sasso, G., Celli, N., Caboni, M., Murzilli, S., Salvatore, L., Morgano, A., Vacca, M., Pagliani, T., Parini, P., and Moschetta, A. (2010). Down-regulation of the LXR transcriptome provides the requisite cholesterol levels to proliferating hepatocytes. Hepatology *51*, 1334-1344. 10.1002/hep.23436.

31. Willy, P.J., Umesono, K., Ong, E.S., Evans, R.M., Heyman, R.A., and Mangelsdorf, D.J. (1995). LXR, a nuclear receptor that defines a distinct retinoid response pathway. Genes & development *9*, 1033-1045. 10.1101/gad.9.9.1033.

32. Kyle, S.M., Saha, P.K., Brown, H.M., Chan, L.C., and Justice, M.J. (2016). MeCP2 co-ordinates liver lipid metabolism with the NCoR1/HDAC3 corepressor complex. Hum Mol Genet *25*, 3029-3041. 10.1093/hmg/ddw156.

33. Na, E.S., Nelson, E.D., Kavalali, E.T., and Monteggia, L.M. (2013). The impact of MeCP2 loss- or gain-of-function on synaptic plasticity. Neuropsychopharmacology *38*, 212-219. 10.1038/npp.2012.116.

34. Chen, Z., Li, X., Zhou, J., Yuan, B., Yu, B., Tong, D., Cheng, C., Shao, Y., Xia, S., Zhang, R., et al. (2017). Accumulated quiescent neural stem cells in adult hippocampus of the mouse model for the MECP2 duplication syndrome. Scientific reports *7*. 10.1038/srep41701.

35. Brown, K., Selfridge, J., Lagger, S., Connelly, J., De Sousa, D., Kerr, A., Webb, S., Guy, J., Merusi, C., Koerner, M.V., and Bird, A. (2016). The molecular basis of variable phenotypic severity among common missense mutations causing Rett syndrome. Human molecular genetics *25*, 558-570. 10.1093/hmg/ddv496.

36. Ausio, J., Martinez de Paz, A., and Esteller, M. (2014). MeCP2: the long trip from a chromatin protein to neurological disorders. Trends Mol Med *20*, 487-498. 10.1016/j.molmed.2014.03.004.
37. Lamonica, J.M., Kwon, D.Y., Goffin, D., Fenik, P., Johnson, B.S., Cui, Y., Guo, H., Veasey, S., and Zhou, Z. (2017). Elevating expression of MeCP2 T158M rescues DNA binding and Rett syndrome-like phenotypes. J Clin Invest *127*, 1889-1904. 10.1172/JCI90967.
38. Bellini, E., Pavesi, G., Barbiero, I., Bergo, A., Chandola, C., Nawaz, M.S., Rusconi, L., Stefanelli, G., Strollo, M., Valente, M.M., et al. (2014). MeCP2 post-translational modifications: a mechanism to control its involvement in synaptic plasticity and homeostasis? Frontiers in cellular neuroscience *8*, 236. 10.3389/fncel.2014.00236.
39. Wang, Y. (2014). RING finger protein 4 (RNF4) derepresses gene expression from DNA methylation. The Journal of biological chemistry *289*, 33808-33813. 10.1074/jbc.C114.611558.
40. Coller, H.A. (2019). The paradox of metabolism in quiescent stem cells. FEBS letters *593*, 2817-2839. 10.1002/1873-3468.13608.
41. Liu, M., and Chen, P. (2017). Proliferation□inhibiting pathways in liver regeneration (Review). Mol Med Rep *16*, 23-35. 10.3892/mmr.2017.6613.
42. Rudraiah, S., Zhang, X., and Wang, L. (2016). Nuclear Receptors as Therapeutic Targets in Liver Disease: Are We There Yet? Annual review of pharmacology and toxicology *56*, 605-626. 10.1146/annurev-pharmtox-010715-103209.
43. Pearen, M.A., and Muscat, G.E. (2012). Orphan nuclear receptors and the regulation of nutrient metabolism: understanding obesity. Physiology *27*, 156-166. 10.1152/physiol.00007.2012.
44. Zheng, Y., and Murphy, L.C. (2016). Regulation of steroid hormone receptors and coregulators during the cell cycle highlights potential novel function in addition to roles as transcription factors. Nucl Recept Signal *14*, e001. 10.1621/nrs.14001.
45. Zhao, P., Fan, S., Gao, Y., Huang, M., and Bi, H. (2022). Nuclear Receptor-Mediated Hepatomegaly and Liver Regeneration: An Update. Drug metabolism and disposition: the biological fate of chemicals *50*, 636-645. 10.1124/dmd.121.000454.
46. Huang, W., Ma, K., Zhang, J., Qatanani, M., Cuvillier, J., Liu, J., Dong, B., Huang, X., and Moore, D.D. (2006). Nuclear receptor-dependent bile acid signaling is required for normal liver regeneration. Science *312*, 233-236. 10.1126/science.1121435.
47. Wallbaum, S., Grau, N., Schmid, A., Frick, K., Neeb, A., and Sleeman, J.P. (2009). Cell cycle quiescence can suppress transcription from an ecdysone receptor-based inducible promoter in mammalian cells. BioTechniques *46*, 433-440. 10.2144/000113121.
48. Jourdren, L., Bernard, M., Dillies, M.A., and Le Crom, S. (2012). Eoulsan: a cloud computing-based framework facilitating high throughput sequencing analyses. Bioinformatics *28*, 1542-1543. 10.1093/bioinformatics/bts165.
49. Li, H., Handsaker, B., Wysoker, A., Fennell, T., Ruan, J., Homer, N., Marth, G., Abecasis, G., Durbin, R., and Genome Project Data Processing, S. (2009). The Sequence Alignment/Map format and SAMtools. Bioinformatics *25*, 2078-2079. 10.1093/bioinformatics/btp352.
50. Pertea, M., Kim, D., Pertea, G.M., Leek, J.T., and Salzberg, S.L. (2016). Transcript-level expression analysis of RNA-seq experiments with HISAT, StringTie and Ballgown. Nature protocols *11*, 1650-1667. 10.1038/nprot.2016.095.
51. Love, M.I., Huber, W., and Anders, S. (2014). Moderated estimation of fold change and dispersion for RNA-seq data with DESeq2. Genome Biol *15*, 550. 10.1186/s13059-014-0550-8.
52. Bolger, A.M., Lohse, M., and Usadel, B. (2014). Trimmomatic: a flexible trimmer for Illumina sequence data. Bioinformatics *30*, 2114-2120. 10.1093/bioinformatics/btu170.

53. Langmead, B., and Salzberg, S.L. (2012). Fast gapped-read alignment with Bowtie 2. Nat Methods *9*, 357-359. 10.1038/nmeth.1923.

54. Zhang, Y., Liu, T., Meyer, C.A., Eeckhoute, J., Johnson, D.S., Bernstein, B.E., Nusbaum, C., Myers, R.M., Brown, M., Li, W., and Liu, X.S. (2008). Model-based analysis of ChIP-Seq (MACS). Genome biology *9*, R137. 10.1186/gb-2008-9-9-r137.

55. Heinz, S., Benner, C., Spann, N., Bertolino, E., Lin, Y.C., Laslo, P., Cheng, J.X., Murre, C., Singh, H., and Glass, C.K. (2010). Simple combinations of lineage-determining transcription factors prime cis-regulatory elements required for macrophage and B cell identities. Molecular cell *38*, 576-589. 10.1016/j.molcel.2010.05.004.

56. Ramirez, F., Ryan, D.P., Gruning, B., Bhardwaj, V., Kilpert, F., Richter, A.S., Heyne, S., Dundar, F., and Manke, T. (2016). deepTools2: a next generation web server for deep-sequencing data analysis. Nucleic acids research *44*, W160-165. 10.1093/nar/gkw257.

57. Cao, T., Chen, H., Huang, W., Xu, S., Liu, P., Zou, W., Pang, M., Xu, Y., Bai, X., Liu, B., et al. (2022). hUC-MSC-mediated recovery of subacute spinal cord injury through enhancing the pivotal subunits beta3 and gamma2 of the GABA(A) receptor. Theranostics *12*, 3057-3078. 10.7150/thno.72015.